symmetry

MDPI

Article

Asymmetry and Symmetry in New Three-Dimensional Chaotic Map with Commensurate and Incommensurate Fractional Orders

Hussein Al-Taani [1], Ma'mon Abu Hammad [2], Mohammad Abudayah [1], Louiza Diabi [3,*] and Adel Ouannas [4]

[1] School of Electrical Engineering and Information Technology, German Jordanian University, Amman 11180, Jordan; hussein.taani@gju.edu.jo (H.A.-T.); mohammad.abudayah@gju.edu.jo (M.A.)
[2] Department of Mathematics, Al-Zaytoonah University of Jordan, Amman 11733, Jordan; m.abuhammad@zuj.edu.jo
[3] Laboratory of Dynamical Systems and Control, University of Larbi Ben M'hidi, Oum El Bouaghi 04000, Algeria
[4] Department of Mathematics and Computer Sciences, University of Larbi Ben M'hidi, Oum El Bouaghi 04000, Algeria; ouannas.adel@univ-oeb.dz
* Correspondence: louiza.diabi@univ-oeb.dz

Abstract: According to recent research, discrete-time fractional-order models have greater potential to investigate behaviors, and chaotic maps with fractional derivative values exhibit rich dynamics. This manuscript studies the dynamics of a new fractional chaotic map-based three functions. We analyze the behaviors in commensurate and incommensurate orders, revealing their impact on dynamics. Through the maximum Lyapunov exponent (LE_{max}), phase portraits, and bifurcation charts. In addition, we assess the complexity and confirm the chaotic features in the map using the approximation entropy $ApEn$ and C_0 complexity. Studies show that the commensurate and incommensurate derivative values influence the fractional chaotic map-based three functions, which exhibit a variety of dynamical behaviors, such as hidden attractors, asymmetry, and symmetry. Moreover, the new system's stabilizing employing a 3D nonlinear controller is introduced. Finally, our study validates the research results using the simulation MATLAB R2024a.

Keywords: symmetry–asymmetry; chaotic dynamics; functions; discrete fractional calculus; complexity

Citation: Al-Taani, H.; Abu Hammad, M.; Abudayah, M.; Diabi, L.; Ouannas, A. Asymmetry and Symmetry in New Three-Dimensional Chaotic Map with Commensurate and Incommensurate Fractional Orders. *Symmetry* **2024**, *16*, 1447. https://doi.org/10.3390/sym16111447

Academic Editors: Cristian Lazureanu and Dana Constantinescu

Received: 30 September 2024
Revised: 14 October 2024
Accepted: 16 October 2024
Published: 31 October 2024

1. Introduction

Sigmoidal-based maps with non-integer and integer orders have newly been suggested [1–3]. Over the last few years, sigmoidal functions have attracted a lot of interest from researchers and have advanced a number of fields, including neuromorphic systems [4], computing [5], and secure communication [6]. Their ability to smoothly transition between two asymptotic values, along with the coexistence of attractors and multiple stability, makes them useful in dynamic chaotic maps.

In the field of fractional order, researchers' focus has shifted to discrete chaotic systems with fractional order and their applications [7]. Moreover, sensitivity to alterations in fractional orders, as well as small perturbations in initial conditions and parameters, is one of the unique advantages of fractional derivative maps. In addition, the rich dynamics and simple forms of fractional maps make them useful for numerical computation and system analysis. Topics covered in fractional calculus include fractional derivatives and fractional difference operators. Nevertheless, because of its outstanding applications in numerous domains, this field has only recently undergone extensive and intense exploration [8]. Khennaoui et al. [9] presented additional evidence for chaotic attractors in the Stefanski, Wang, and Rössler fractional maps. Upon searching for chaos events in dynamical systems, a great deal of work has been conducted to completely investigate the behaviors of fractional and classical maps [10]. Moreover, the creation of pseudorandom sequences and improved data encryption are made possible by the chaotic systems' randomness, unpredictability,

and sensitivity to initial conditions [11,12]. The intrinsic benefits of chaotic behaviors have led to notable advancements in a number of domains, such as data encryption, secure communications, picture and signal processing, optimization methods, and others. Chaotic maps include many intricate dynamic phenomena, including multistability, bifurcation, coexisting attractors, and hidden attractors [13].

In the literature on chaos, the analysis of chaotic fractional maps without equilibrium has received a lot of attention up to this point because of its usefulness in engineering systems. These systems' associated attractors are referred to as "hidden attractors". Nonlinear systems without a fixed point, those with line-fixed points, and nonlinear systems with just stable points all exhibit these types of attractors [14]. The mathematical representation of real-life system occurrences is demonstrated to benefit from the concepts and implementation of these systems. There are not many studies on "hidden attractors" in chaotic maps. Currently, there are a few published manuscripts on this discussion topic. Both the approximation entropy computation and the complexity test have been used to show that chaotic hidden attractors exist in system dynamics. Later, a fractional map's intricate dynamic with hidden attractors was studied using bifurcation charts, maximum Lyapunov exponents, and complexity in these two references [15,16]. Additionally, a great deal of study has been carried out on the control and synchronization of such types of systems [17–20]. This has led us to investigate the issue and create suitable control fundamentals for coexisting types. Jiang et al. [17] examined the bidirectional coupling problem for N-coupled fractional-order chaotic systems with ring connection synchronization, whereas [18] studied N-coupled fractional-order complex chaotic systems with ring connection synchronization and antisynchronization. Chen et al. [19] analyzed multiple chaotic systems with uncertainty and disturbances synchronized via sliding mode. In [20] tackling stabilizing sampled data for nonlinear chaotic models. However, based on the selected fractional values, such as commensurate and incommensurate orders, these studies have shown that the system's behaviors are complex, with coexisting chaos [21]; specifically, Hamadneh et al. discussed the commensurate and incommensurate orders of the new chaotic model and analyzed its behaviors in these two cases. For future research on fractional dynamics, this area presents an intriguing direction [22].

Recently, research on symmetry and asymmetry maps has been ongoing in order to find new uses and comprehend complex dynamics, as they are useful in the analysis of chaotic maps [23–25]. In reference [23], Elaskar discussed symmetry and chaos in the behavior of nonlinear systems. Meanwhile, [24] explored symmetry-based modulation in a chaotic communication model by Karimov et al. Additionally, in [25], constructed a three-dimensional chaotic system based on conditional symmetry. The traits that draw attention in chaotic maps include asymmetric and symmetry coexisting bifurcations and multistability. For example, in [26], Pratiwi et al. introduce the best model of artificial neural networks using sigmoid. Yang et al. [27] designed rotationally multiwing symmetric models that have either no equilibrium point or just stable equilibria. Encryption and asymmetric chaotic memristor-coupled neural networks were investigated by Lin et al. [28]. In [29], novel research directions regarding artificial neural networks are suggested by memristive neural networks. This work seeks to advance the field by presenting a novel fractional chaotic map based on three functions. Among the unique features of the designed systems is the coexistence of several chaotic hidden attractors. Through numerical techniques, our study opens up new avenues for research and practical applications in the domains of nonlinear dynamics and chaos theory.

The manuscript is organized in the following manner: Section 2 offers a few preliminary on fractional calculus and a new fractional chaotic map based on three functions, demonstrating the asymmetry and absence of fixed points. In Section 3, the analysis of the nonlinear dynamics is illustrated, focusing on commensurate- and incommensurate-order scenarios through the highest Lyapunov exponents, bifurcation plots, and phase portraits applied to illuminate the intricate behavior of the created map. In Section 4, a complexity test, such as $ApEn$, and C_0 complexity are employed to verify and quantify the complexity

of the chaos in the novel model. In Section 5, the nonlinear stability controller is proposed, aimed at forcing the map to converge asymptotically towards zero points. The results of our study are summarized in Section 6, along with ideas for future research.

2. Basic Concepts and Fractional Order Map

To explain our framework, we first give an overview of discrete fractional calculus. Specifically, the goal of this research is to build a new fractional chaotic map based on three functions using a Caputo-like operator.

2.1. Fractional Discrete Operators

This part goes over some of the basic concepts and terminology concerning the Caputo-like operator.

Definition 1 ([30]). *The fractional sum* $\Delta_t^{-\mathrm{Y}}$ *is defined as*

$$\Delta_t^{-\mathrm{Y}}\psi(s) = \frac{1}{\Gamma(\mathrm{Y})}\sum_{l=\mathrm{Y}}^{s-\mathrm{Y}}(s-\varepsilon-1)^{(\mathrm{Y}-1)}\psi(\varepsilon), \quad \mathrm{Y}>0, s\in(\mathbb{N})_{t+\mathrm{Y}}. \tag{1}$$

Definition 2 ([31]). *The* Y*-th Caputo-like difference operator* ${}^{\mathrm{C}}\Delta_t^{\mathrm{Y}}$ *is characterized as*

$$\begin{aligned} {}^{\mathrm{C}}\Delta_t^{\mathrm{Y}}\psi(s) &= \Delta_t^{-(\varepsilon-\mathrm{Y})}\Delta^{\varepsilon}\psi(s) \\ &= \frac{1}{\Gamma(\varepsilon-\mathrm{Y})}\sum_{s=t}^{s-(\varepsilon-\mathrm{Y})}(s-\varepsilon-1)^{(\varepsilon-\mathrm{Y}-1)}\Delta^{\varepsilon}\psi(s). \end{aligned} \tag{2}$$

$s\in(\mathbb{N})_{t-\mathrm{Y}+\varepsilon}$ *and* $l=\lceil \mathrm{Y}\rceil+1$. *The falling factorial function* $(s-\varepsilon-1)^{(\varepsilon-\mathrm{Y}-1)}$ *and the* Y^{th}*-integer differences operator* $\Delta^{\mathrm{Y}}\psi(s)$ *have the following expressions:*

$$\Delta^{\varepsilon}\psi(s) = \Delta(\Delta^{\varepsilon-1}\psi(s)) = \sum_{t=0}^{\varepsilon}\binom{\ell}{t}(-1)^{\varepsilon-t}\psi(s+t), \tag{3}$$

and

$$(s-1-\varepsilon)^{(\varepsilon-\mathrm{Y}-1)} = \frac{\Gamma(s-l)}{\Gamma(s+1-\varepsilon-t+\mathrm{Y})}. \tag{4}$$

The following theorem is next applied to attain the numerical formula for fractional discrete systems.

Theorem 1 ([32]). *The solution of the following system*

$$\begin{cases} {}^{\mathrm{C}}\Delta_t^{\mathrm{Y}}\psi(s) = g(s-1+\mathrm{Y},\psi(s+\mathrm{Y}-1)) \\ \Delta^{\jmath}\psi(s) = \psi_{\jmath}, \quad \varepsilon = \lceil \mathrm{Y}\rceil+1, \quad \jmath = 0,1,\ldots,\varepsilon-1, \end{cases} \tag{5}$$

is given by

$$\psi(s) = \psi_0(t) + \frac{1}{\Gamma(\mathrm{Y})}\sum_{l=t+s-\mathrm{Y}}^{s-\mathrm{Y}}(s-\varepsilon)^{(\mathrm{Y}-1)}g(\varepsilon+\mathrm{Y}-1,\psi(\varepsilon+\mathrm{Y}-1)), \quad s\in\mathbb{N}_{t+\varepsilon}, \tag{6}$$

where

$$\psi_0(t) = \sum_{\jmath=0}^{\varepsilon-1}\frac{(s-t)^{\jmath}}{\Gamma(\jmath+1)}\Delta^{\jmath}\psi(t). \tag{7}$$

Take $t=0$, $\jmath=\mathrm{Y}-1+\varepsilon$, $s=1$ and for $\mathrm{Y}\in(0,1]$, $(s-\varepsilon-1)^{(\mathrm{Y}-1)} = \frac{\Gamma(s-\varepsilon)}{\Gamma(s-\varepsilon-\mathrm{Y}+1)}$. The way to write numerical formula (6) is as follows:

$$\psi(s) = \psi(0) + \frac{1}{\Gamma(\Upsilon)} \sum_{\jmath=0}^{s-1} \frac{\Gamma(s-\jmath+\Upsilon-1)}{\Gamma(s-\jmath)} g(\jmath, \psi(\jmath)). \tag{8}$$

2.2. A Three-Dimensional Fractional Map

The sigmoidal function is known to be capable of approaching -1 and 1, which changes an input into an output, especially since they are known for their distinctive nonlinear behavior and capacity to modify data. Moreover, quadratic and absolute value functions have been proposed by researchers utilizing differential modeling theories $(x_3(n))^2 - 1$ and $\eta|x_2(n)| - 1$, respectively. In [33,34], the dynamics of discrete-time integer-order system-based various functions were explored, which are known for their distinctive nonlinear behavior and capacity to change data, where the sigmoidal function is defined by $F(x) = \frac{1}{1+e^{-\beta x_1(n)}}$. The S-shaped curve of the sigmoidal function and initial-relied pinched hysteresis loops of quadratic and absolute value maps illustrated in Figure 1 demonstrate the nonlinear sigmoidal function input values into a limited range, while other functions generate a hysteresis loop.

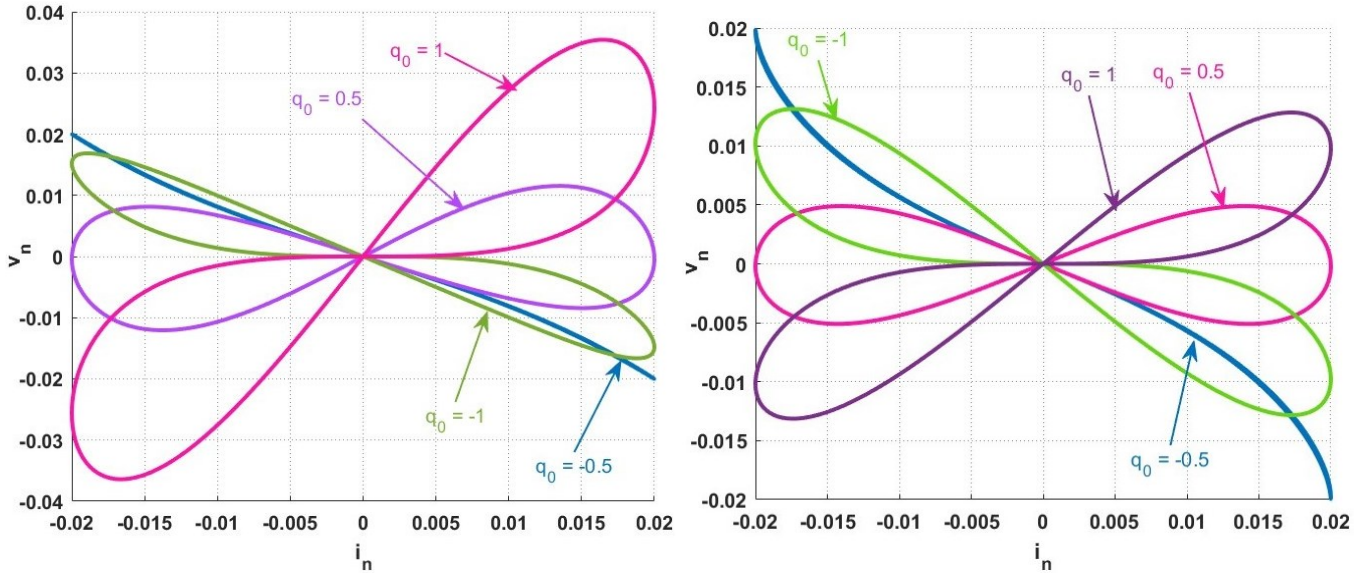

(**a**) Quadratic hysteresis loops (**b**) Absolute value hysteresis loops

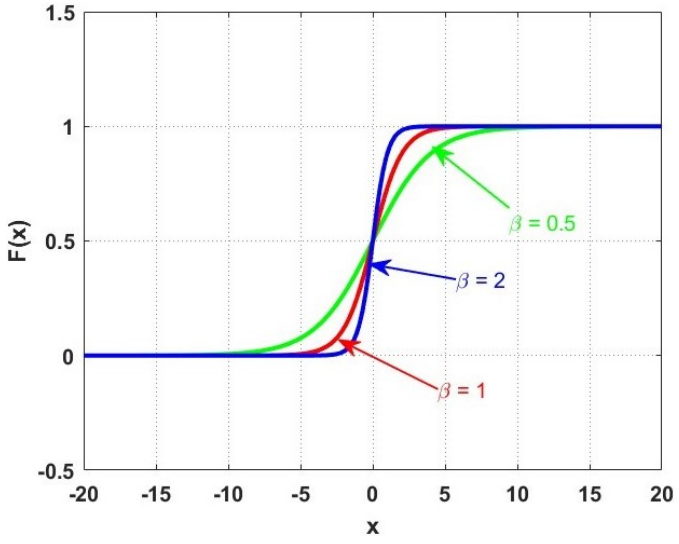

(**c**) Sigmoidal curve

Figure 1. (**a**,**b**) Initial-relied pinched hysteresis loops, (**c**) S-shaped sigmoidal function.

Through this paper, we produce new fractional chaotic map-based three functions, using the difference operator ${}^{C}\Delta_{t}^{Y_i}$, represented by 3D fractional difference equations as follow:

$$\begin{cases} {}^{C}\Delta_{t}^{Y} x_1(s) = \dfrac{\sigma_1}{1+e^{-\beta x_1(\theta)}} + \sigma_2\sigma_3 x_1(\theta)(\eta|x_2(\theta)|-1)((x_3(\theta))^2-1) \\ \qquad\qquad - x_1(\theta), \\ {}^{C}\Delta_{t}^{Y} x_2(s) = x_1(\theta), \\ {}^{C}\Delta_{t}^{Y} x_3(s) = \sigma_2 x_1(\theta)(\eta|x_2(\theta)|-1), \end{cases} \tag{9}$$

where $\theta = s - 1 + Y$, σ_1, and β are the controller parameters of the sigmoidal function, σ_2 and η are the controller parameters of absolute value, and σ_3 is the controller parameter of quadratic maps. The equilibrium points (EP) $(x_1^*, x_2^*, x_3^*,)$ of the new fractional chaotic map-based three functions (9) can be determined by solving the following:

$$\begin{cases} \dfrac{\sigma_1}{1+e^{-\beta x_1^*}} + \sigma_2\sigma_3 x_1^*(\eta|x_2^*|-1)((x_3^*)^2-1)) - x_1^* = 0, \\ x_1^* = 0, \\ \sigma_2 x_1^*(\eta|x_2^*|-1) = 0. \end{cases} \tag{10}$$

Clearly, from Equation (2) of (10), $x_1^* = 0$, replacing x_1^* in Equatios (1) and (3), when $\sigma_1 \neq 0$ the system (10), there are no (EP). Then, every attractor of the new fractional chaotic map-based three functions (9) are hidden and show asymmetry if $\sigma_1 \neq 0$, as displayed in Figure 2.

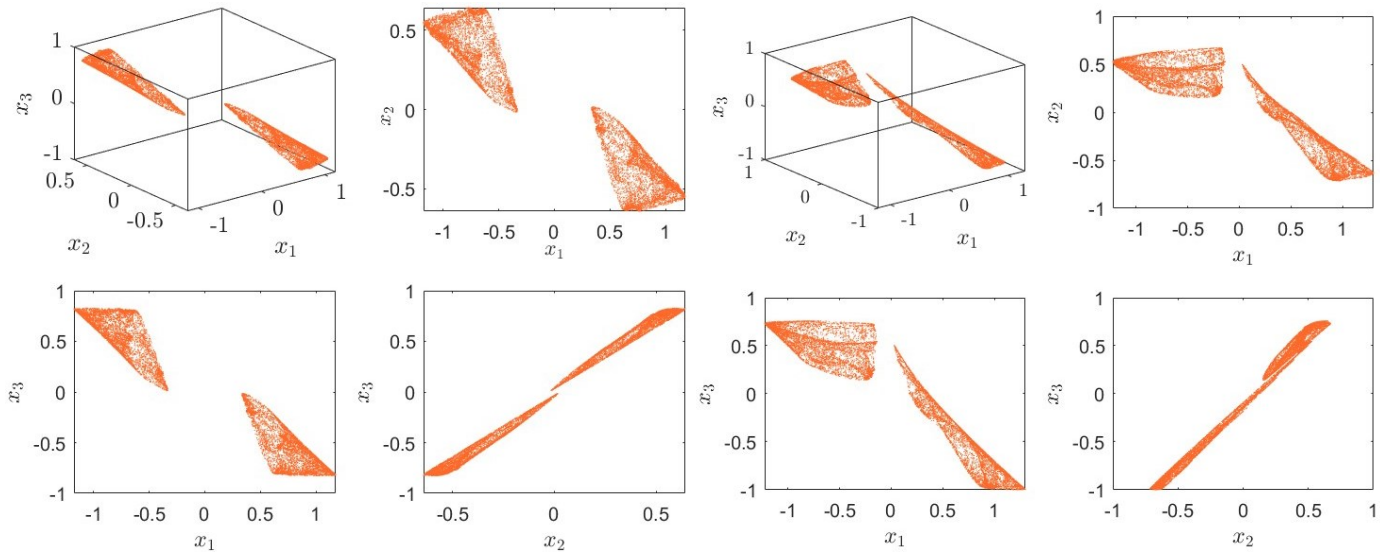

(**a**) $\sigma_1 = 0$ (**b**) $\sigma_1 \neq 0$

Figure 2. (**a**) Symmetry for $\sigma_1 = 0$, $\beta = 1$, $\sigma_2 = -1.7$, $\sigma_3 = 1.15$, and $\eta = 0.35$. (**b**) Asymmetry for $\sigma_1 = -0.2$, $\beta = 1$, $\sigma_2 = -1.7$, $\sigma_3 = 1.15$, and $\eta = 0.35$.

3. Bifurcation and Hidden Chaos

Here, the behaviors of the new fractional chaotic map-based three functions (9) are analyzed. We conduct the analysis in both commensurate and incommensurate orders. Various numerical tools are utilized, including phase portrait visualization, bifurcation illustration, and maximum Lyapunov exponent (LE_{max}) estimation.

3.1. The Commensurate-Order Case

The focus of this subsection is studying the dynamics of the new fractional chaotic map-based three functions (9) under commensurate order. It is crucial to understand that equations with the same orders constitute a commensurate-order fractional map. We describe the numerical formula of (9) based on Theorem 1 in the following manner:

$$\begin{cases} x_1(s) = x_1(0) + \frac{1}{\Gamma(\Upsilon)} \sum\limits_{j=0}^{s} \frac{\Gamma(s-1+\Upsilon-j)}{\Gamma(s-j)} \Big(\frac{\sigma_1}{1+e^{-\beta x_1(j)}} + \sigma_2\sigma_3 x_1(j)(\eta|x_2(j)|-1)((x_3(j))^2-1) - x_1(j) \Big), \\ x_2(s) = x_2(0) + \frac{1}{\Gamma(\Upsilon)} \sum\limits_{j=0}^{s} \frac{\Gamma(s-1+\Upsilon-j)}{\Gamma(s-j)} (x_1(j)), \\ x_3(s) = x_3(0) + \frac{1}{\Gamma(\Upsilon)} \sum\limits_{j=0}^{s} \frac{\Gamma(s-1+\Upsilon-j)}{\Gamma(s-j)} (\sigma_2 x_1(j)(\eta|x_2(j)|-1)). \quad s = 1,2,3,\cdots \end{cases} \tag{11}$$

We ascertain the LE_{max} of the fractional map using the Jacobin matrix approach [35], so the J_ς is define by

$$J_\varsigma = \begin{pmatrix} W_1(\varsigma) & W_2(\varsigma) & W_3(\varsigma) \\ V_1(\varsigma) & V_2(\varsigma) & V_3(\varsigma) \\ R_1(\varsigma) & R_2(\varsigma) & R_3(\varsigma) \end{pmatrix}, \tag{12}$$

where

$$\begin{cases} W_i(\varsigma) = & W_i(0) + \frac{1}{\Gamma(\Upsilon)} \sum\limits_{j=0}^{\varsigma-1} \frac{\Gamma(\Upsilon+\varsigma-j-1)}{\Gamma(\varsigma-j)} \Big((\frac{\beta\sigma_1 e^{-\beta x_1(j)}}{(1+e-\beta x(j))^2)} + \sigma_2\sigma_3(\eta|x_2(j)|-1)((x_3(j))^2-1))W_i(j) \\ & +(\eta\sigma_2\sigma_3 x_1(j)((x_3(j))^2-1))V_i(j) + (\sigma_2\sigma_3 x_1(j))(\eta|x_2(j)|-1)(2x_3(j)R_i(j) - W_i(j)) \Big), \\ V_i(\varsigma) = & V_i(0) + \frac{1}{\Gamma(\Upsilon)} \sum\limits_{j=0}^{\varsigma-1} \frac{\Gamma(\Upsilon+\varsigma-j-1)}{\Gamma(\varsigma-j)} \Big(W_i(j) \Big), \\ R_i(\varsigma) = & R_i(0) + \frac{1}{\Gamma(\Upsilon)} \sum\limits_{j=0}^{\varsigma-1} \frac{\Gamma(\Upsilon+\varsigma-j-1)}{\Gamma(\varsigma-j)} \Big((\sigma_2(\eta|x_2(j)|-1))W_i(j) + (\eta\sigma_2 x_1(j))V_i(j) \Big), \end{cases} \tag{13}$$

$i = 1,2,3$. Then, for $s = 1,2,3$, the LE_s can be given by

$$LE_s = \lim_{\varsigma\to\infty} \frac{1}{\varsigma} \ln|\lambda_s^{(\varsigma)}|, \quad \text{for} \tag{14}$$

where $\lambda_s^{(\varsigma)}$ are the eigenvalues of J_ς.

Set $\sigma_1 = -0.2$, $\sigma_2 = -1.7$, and $\sigma_3 = 1.15$, $(x_1(0), x_2(0), x_3(0)) = (0.01, 0.01, 0.01)$, $\beta = 1$, $\eta = 0.35$, and (IN), to better understand the impact of commensurate derivative orders on the dynamics of the new fractional chaotic map-based three functions (9); we alter the values of the commensurate orders Υ such that the chaotic region expands. In Figure 3, we created charts of the bifurcation, as well as the associated plots LE_{max} versus $\Upsilon \in [0.65, 1]$; when Υ decreases, the map shows a divergence towards infinity. On the other hand, this indicates that the states become completely chaotic in $[0.88, 1]$, where the LE_{max} are positive.

Now, Figure 4 portrays the bifurcation charts for the commensurate values $\Upsilon = 0.85$ when the controller parameters are $\sigma_1 \in [-0.6, 0.8]$, $\sigma_2 \in [-2, 0]$,$\sigma_3 \in [0, 1.2]$, $\eta \in [0.2, 1.4]$. We can see that the states of the three commensurate map-based functions (9) change the dynamics from periodic to totally chaotic and show a divergence in the motion of infinity in some points. Additionally, Figure 5 displays the LE_{max} that was computed with MATLAB R2024a code, confirming the outcomes of the bifurcation displayed in Figure 4. This indicates non-chaotic behavior, since the $LEmax$ values are negative. In contrast, when the $LEmax$ values are positive, the map displays a chaotic region. It is apparent that the behaviors of the three commensurate map-based functions (9) are influenced by the system factors, and variations in the commensurate derivative Υ have an influence on the rich dynamics of the map (9).

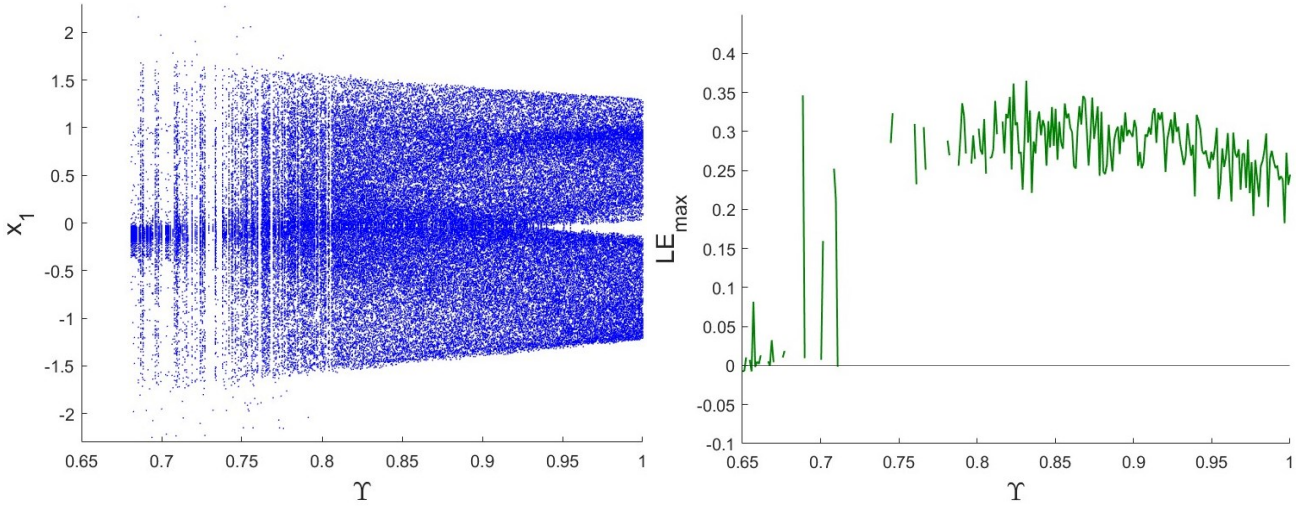

(**a**) (**b**)

Figure 3. (**a**) Bifurcation of (9) for Y $\in [0.65, 1]$. (**b**) The associated LE_{max}.

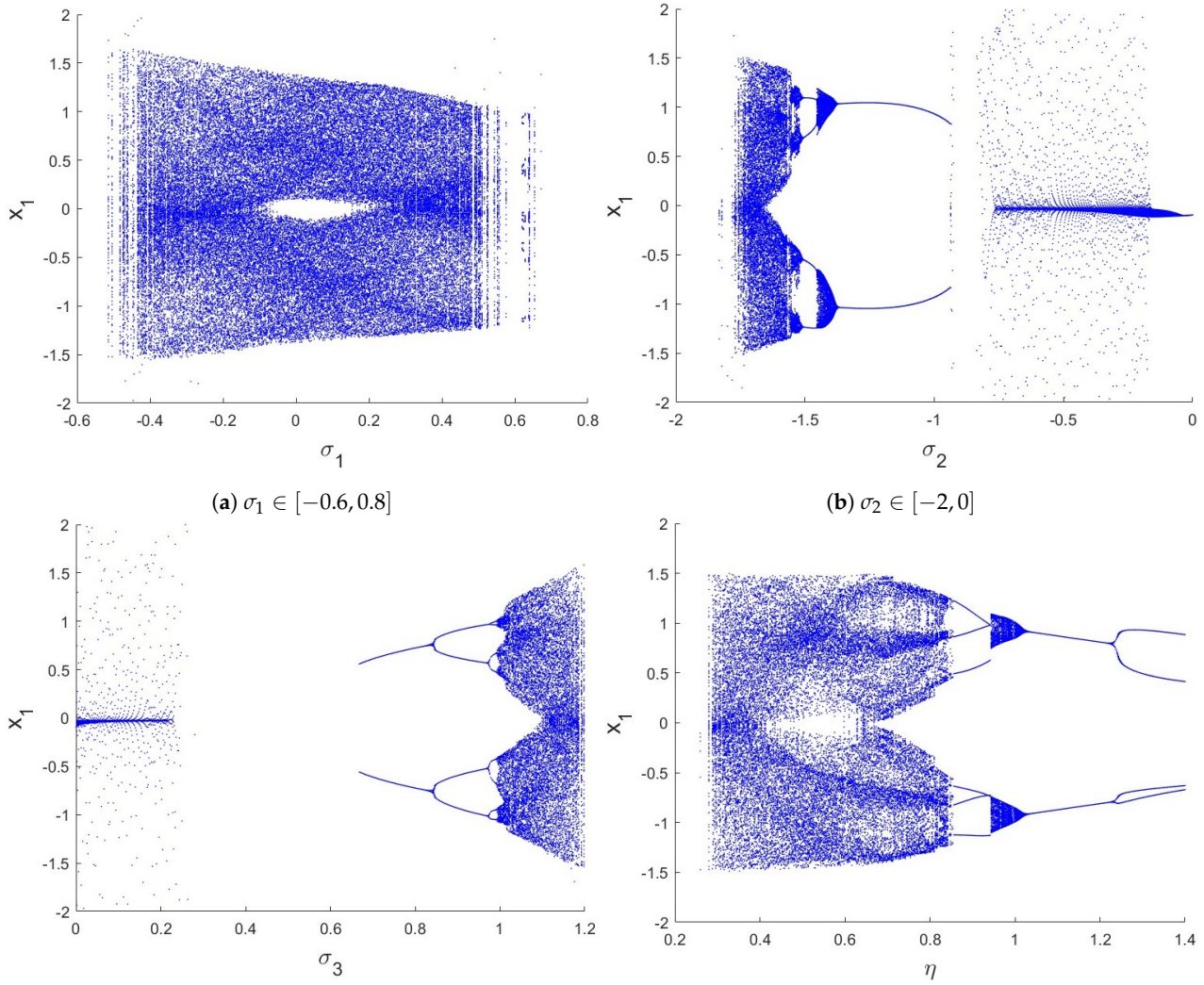

(**a**) $\sigma_1 \in [-0.6, 0.8]$ (**b**) $\sigma_2 \in [-2, 0]$

(**c**) $\sigma_3 \in [0, 1.2]$ (**d**) $\eta \in [0.2, 1.4]$

Figure 4. Bifurcation of (9) versus the controller parameters for Y $= 0.85$.

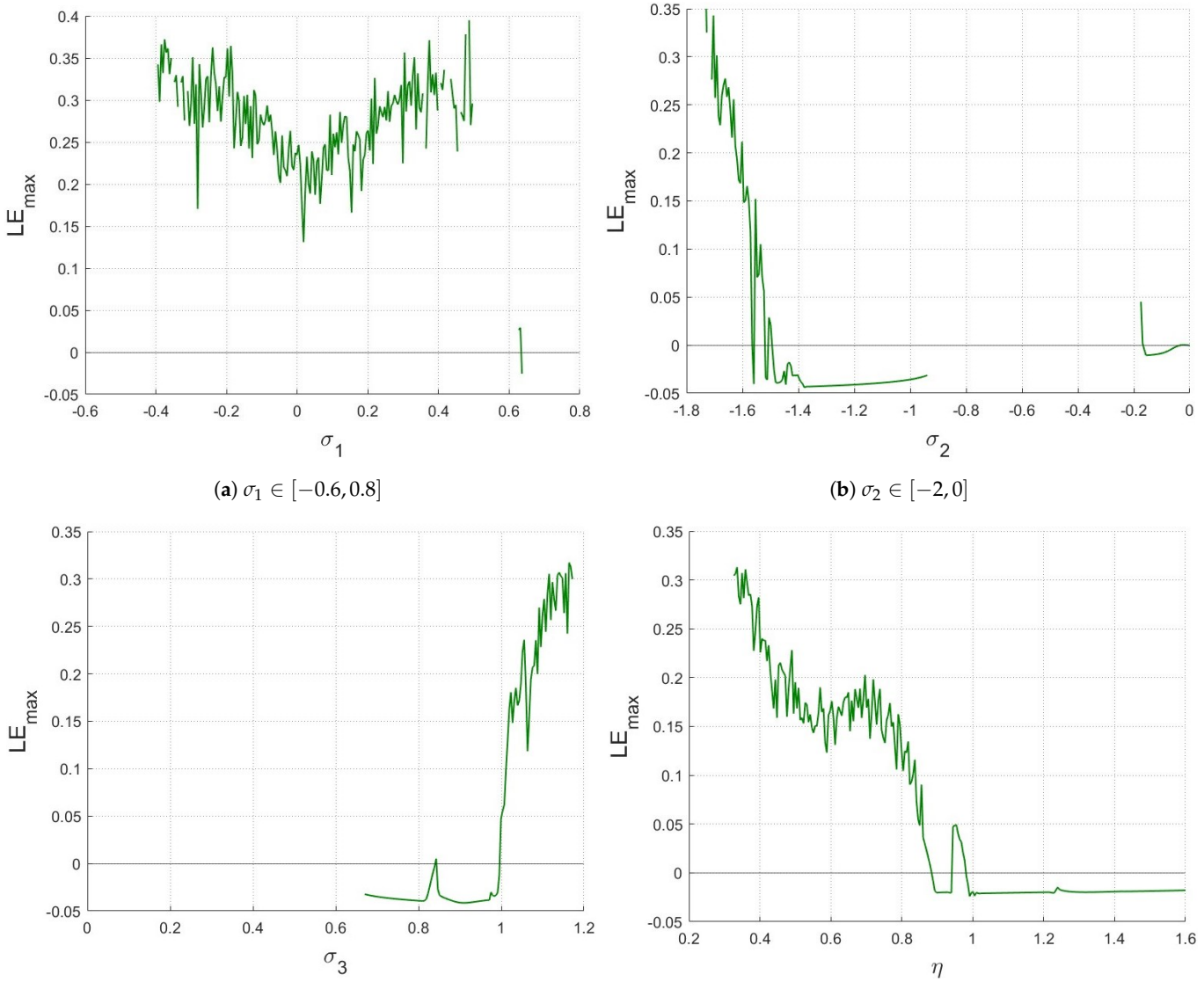

(**a**) $\sigma_1 \in [-0.6, 0.8]$ (**b**) $\sigma_2 \in [-2, 0]$

(**c**) $\sigma_3 \in [0, 1.2]$ (**d**) $\eta \in [0.2, 1.4]$

Figure 5. The LE_{max} of (9) associated with Figure 4 for $\mathrm{Y} = 0.85$.

The evolution states of the three commensurate map-based functions (9) for $\mathrm{Y} = 0.85$ are shown in Figure 6 to be comprehensive. Additionally, Figure 7 illustrates the hidden asymmetry of chaotic attractors for various commensurate orders Y. These results thus demonstrate that commensurate orders determine the hidden attractors form on (9).

3.2. The Incommensurate-Order Case

In the ensuing part, we evaluate the behaviors of the new fractional chaotic map-based three functions with incommensurate order. Using various fractional derivative values for each equation in the map, which is the concept of incommensurate derivative values, leads to the new incommensurate fractional chaotic map-based three functions.

$$\begin{cases} {}^{\mathrm{C}}\Delta_t^{\mathrm{Y}_1} x_1(s) = \dfrac{\sigma_1}{1 + e^{-\beta x_1(\theta_1)}} + \sigma_2\sigma_3 x_1(\theta_1)(\eta|x_2(\theta_1)| - 1)((x_3(\theta_1))^2 \\ \qquad\qquad - 1) - x_1(\theta_1), \\ {}^{\mathrm{C}}\Delta_t^{\mathrm{Y}_2} x_2(s) = x_1(\theta_2), \\ {}^{\mathrm{C}}\Delta_t^{\mathrm{Y}_3} x_3(s) = \sigma_2 x_1(\theta_3)(\eta|x_2(\theta_3)| - 1), \end{cases} \tag{15}$$

where $\theta_1 = s + \mathrm{Y}_1 - 1$, $\theta_2 = s + \mathrm{Y}_2 - 1$, and $\theta_3 = s + \mathrm{Y}_3 - 1$. Based on Theorem 1, we express the following numerical formula of (15):

$$\begin{cases} x_1(s) = x_1(0) + \frac{1}{\Gamma(\mathrm{Y}_1)} \sum\limits_{j=0}^{s} \frac{\Gamma(s-1+\mathrm{Y}_1-j)}{\Gamma(s-j)} \Big(\frac{\sigma_1}{1+e^{-\beta x_1(j)}} + \sigma_2\sigma_3 x_1(j)(\eta|x_2(j)|-1)((x_3(j))^2-1) - x_1(j) \Big), \\ x_2(s) = x_2(0) + \frac{1}{\Gamma(\mathrm{Y}_2)} \sum\limits_{j=0}^{s} \frac{\Gamma(s-1+\mathrm{Y}_2-j)}{\Gamma(s-j)} (x_1(j)), \\ x_3(s) = x_3(0) + \frac{1}{\Gamma(\mathrm{Y}_3)} \sum\limits_{j=0}^{s} \frac{\Gamma(s-1+\mathrm{Y}_3-j)}{\Gamma(s-j)} (\sigma_2 x_1(j)(\eta|x_2(j)|-1)). \quad s = 1, 2, 3, \cdots \end{cases} \tag{16}$$

Firstly, Figure 8 represents the evolution states for the three proposed incommensurate map-based functions (15) when $(\mathrm{Y}_1, \mathrm{Y}_2, \mathrm{Y}_3) = (1, 0.8, 0.9)$, while Figure 9 illustrates the hidden attractors via various incommensurate orders $(\mathrm{Y}_1, \mathrm{Y}_2, \mathrm{Y}_3)$ with (IN).

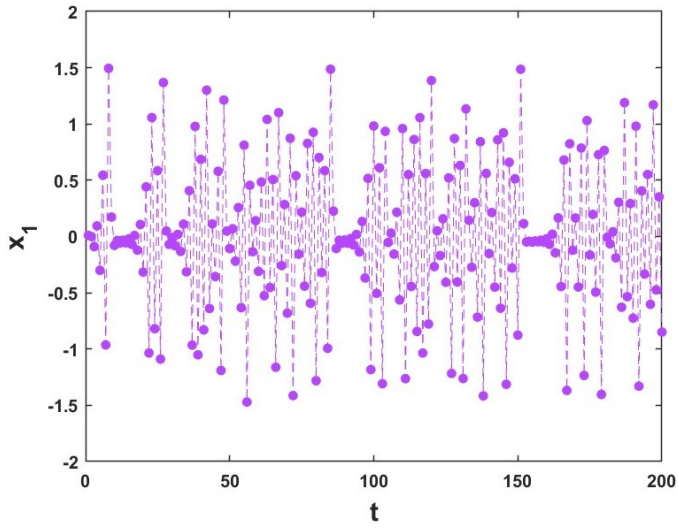

(**a**) Evolution of x_1-t

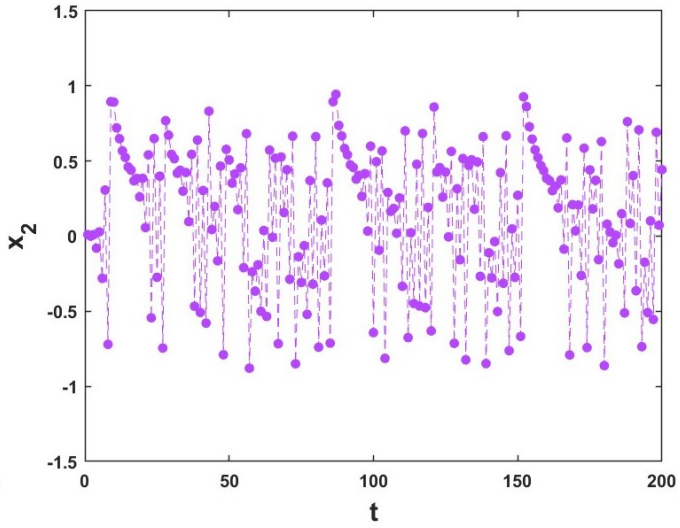

(**b**) Evolution of x_2-t

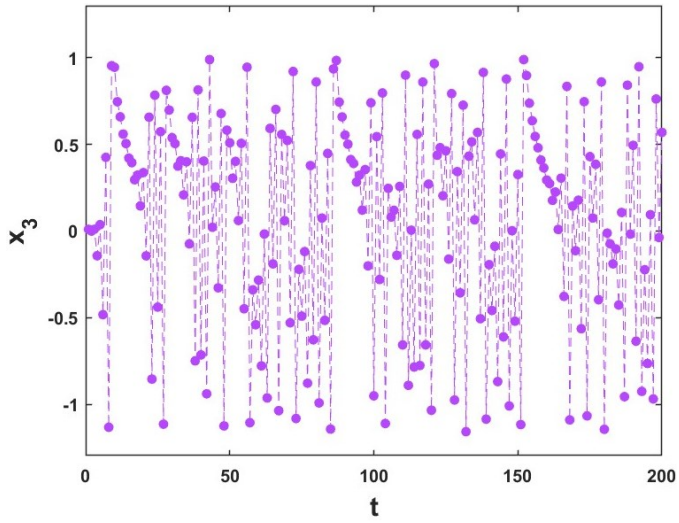

(**c**) Evolution of x_3-t

Figure 6. Time evolution of (9) for $\mathrm{Y} = 0.85$.

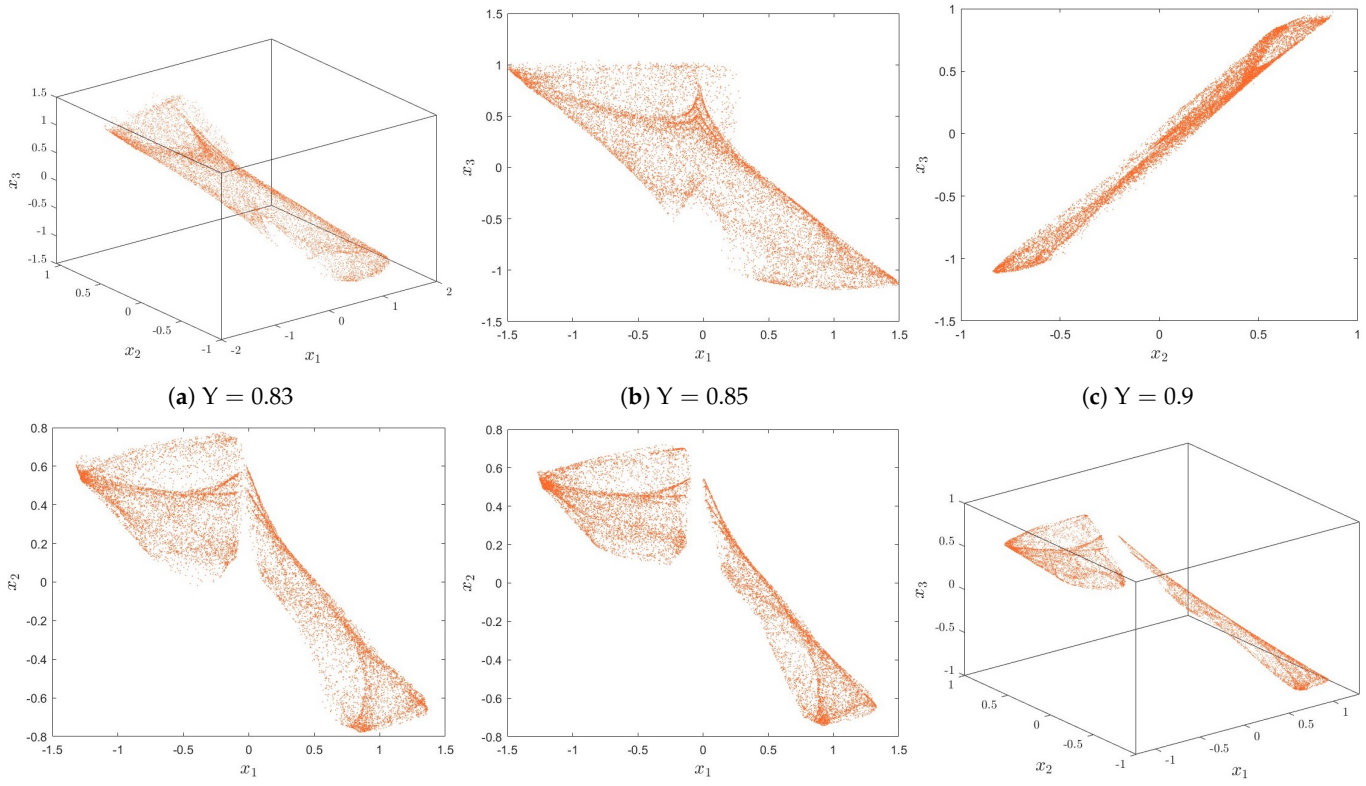

(**a**) Y = 0.83 (**b**) Y = 0.85 (**c**) Y = 0.9

(**d**) Y = 0.95 (**e**) Y = 0.98 (**f**) Y = 1

Figure 7. Hidden attractors of (9) for different Y values.

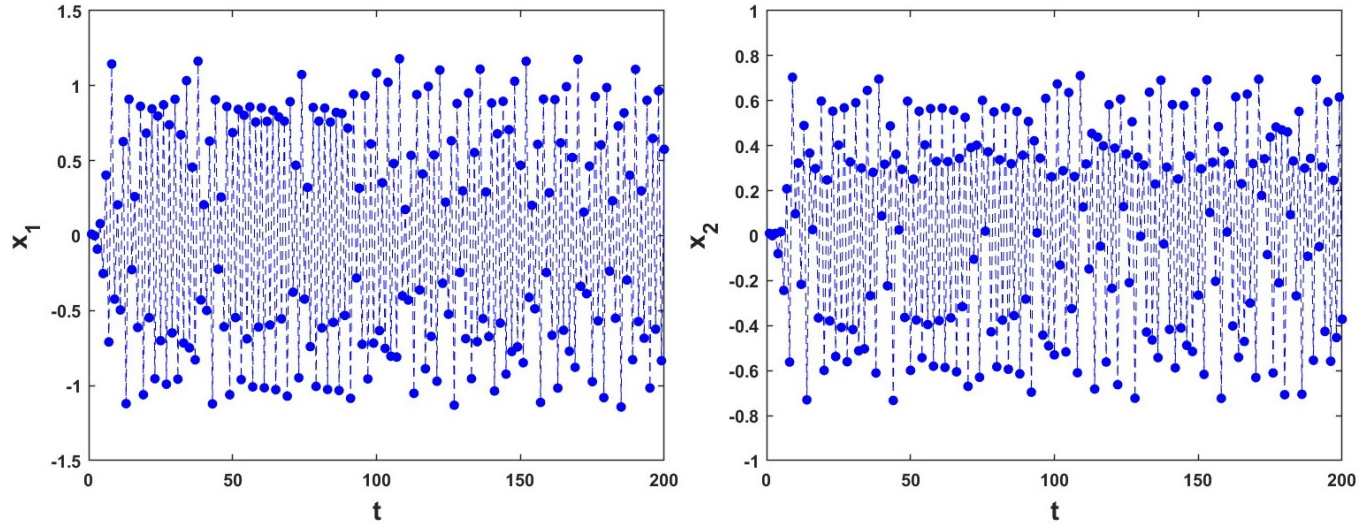

(**a**) Evolution of x_1-t (**b**) Evolution of x_2-t

Figure 8. *Cont.*

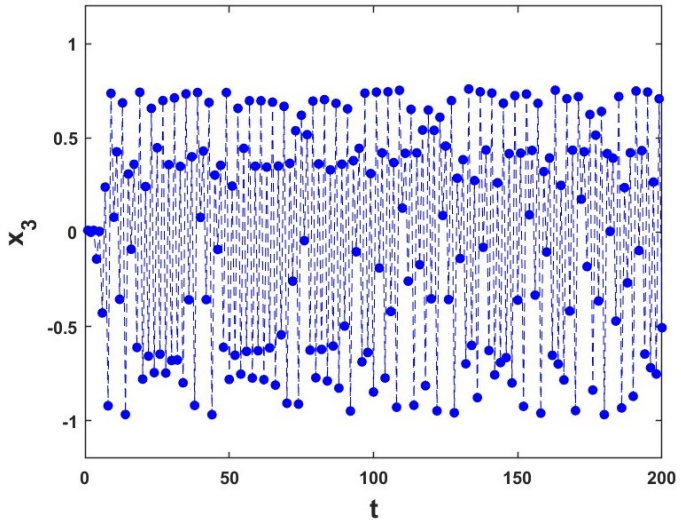

(**c**) Evolution of x_3-t

Figure 8. Time evolution of (15) for $(Y_1, Y_2, Y_3) = (1, 0.8, 0.9)$.

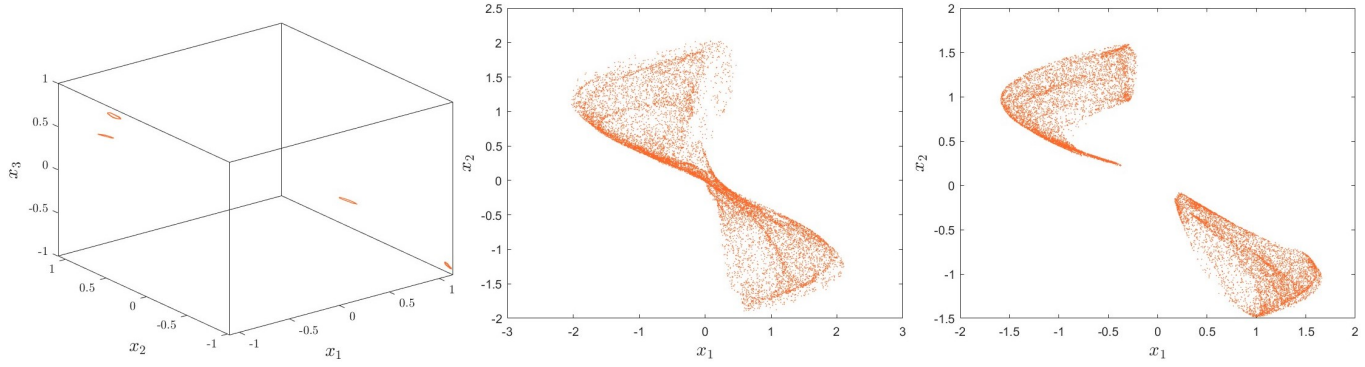

(**a**) $(Y_1, Y_2, Y_3) = (0.9, 0.1, 0.6)$ (**b**) $(Y_1, Y_2, Y_3) = (0.6, 0.1, 0.9)$ (**c**) $(Y_1, Y_2, Y_3) = (0.75, 0.1, 0.9)$

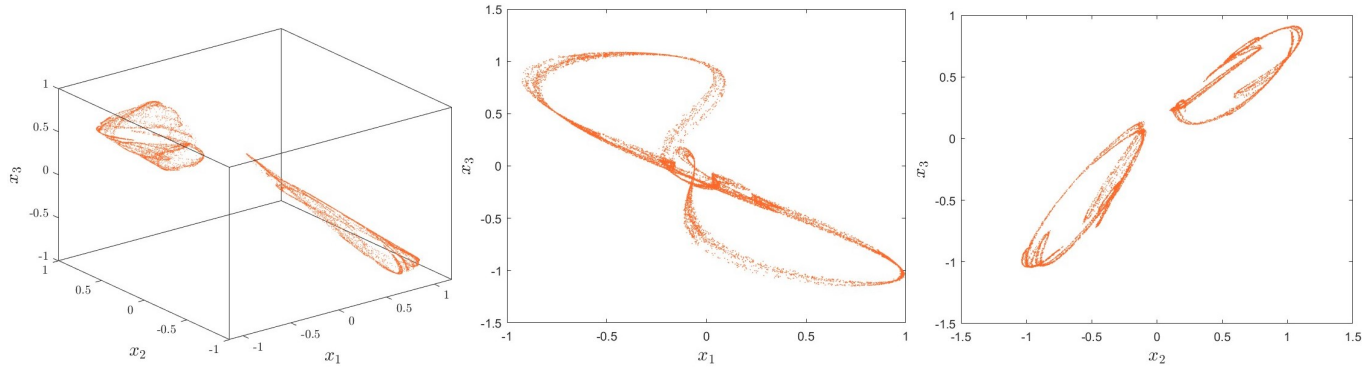

(**d**) $(Y_1, Y_2, Y_3) = (1, 0.8, 0.9)$ (**e**) $(Y_1, Y_2, Y_3) = (0.9, 0.1, 0.2)$ (**f**) $(Y_1, Y_2, Y_3) = (1, 0.5, 0.9)$

Figure 9. Hidden attractors of (15) for different (Y_1, Y_2, Y_3) values.

To comprehend the impact of incommensurate derivative orders on the dynamics of the novel chaotic fractional map-based three functions (15), we created a diagram of the bifurcation, as well as the associated plots $LEmax$ versus the incommensurate-order values Y_1 and Y_2 and Y_3. From Figure 10, $Y_1 \in [0.4, 1]$, and we choose $Y_2 = 0.1$, $Y_3 = 0.9$. We can see that the states exhibit a divergence towards infinity in $[0.4, 0.57]$ and become chaotic in $Y_1 \in [0.58, 0.9]$, where the LE_{max} values are positive, when it increases close to 1 the state become periodic which is evident from the negative values of LE_{max}. Additionally, Figure 11, versus $Y_2 \in (0, 1]$ and fixed the incommensurate derivative by $Y_1 = 1$ and $Y_3 = 0.9$, shows the states of the map are periodic windows appear in $[0, 0.41]$ and chaotic

when $Y_2 \in (0.42, 1]$ through a four period-doubling bifurcation. Furthermore, in Figure 12, we fixed $Y_1 = 0.9$, $Y_2 = 0.1$, and versus Y_3 between 0 and 1; we can see the appearance and disappearance of chaotic behavior within an area of the three proposed incommensurate map-based functions (15). It is observed that the $LEmax$ fluctuates between positive and negative when $Y_3 \in [0, 1]$. Consequently, there are variations in the incommensurate derivative influence the dynamics of (15).

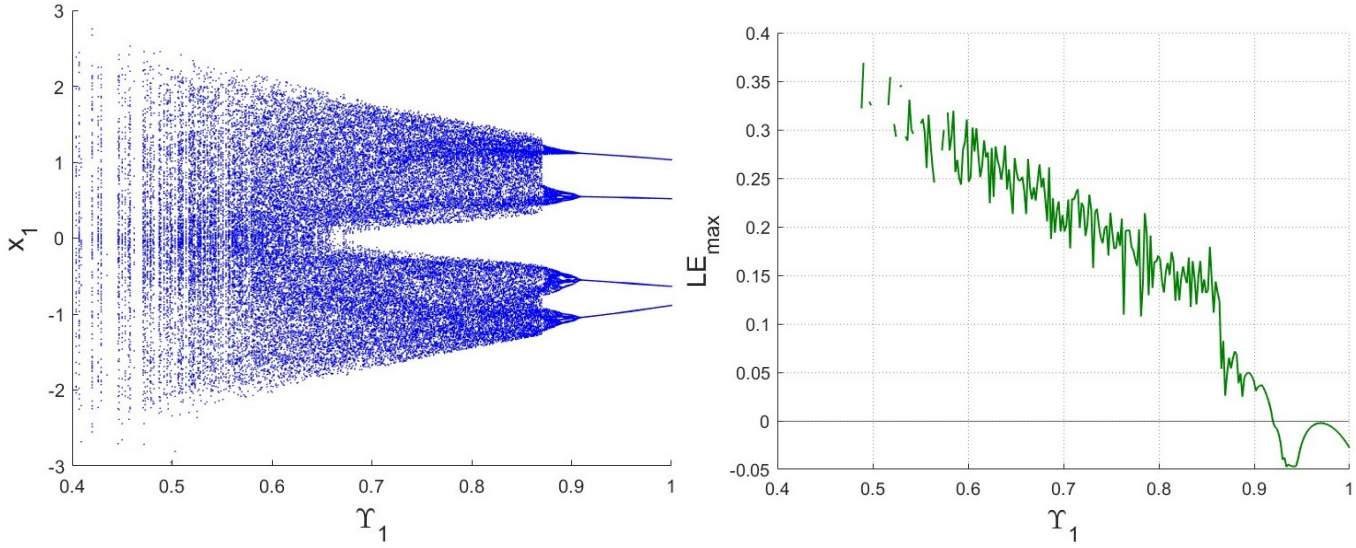

(**a**) (**b**)

Figure 10. (**a**) Bifurcation of (15) for $Y_1 \in [0.4, 1]$, $Y_2 = 0.1$, $Y_3 = 0.9$. (**b**) The associated LE_{max}.

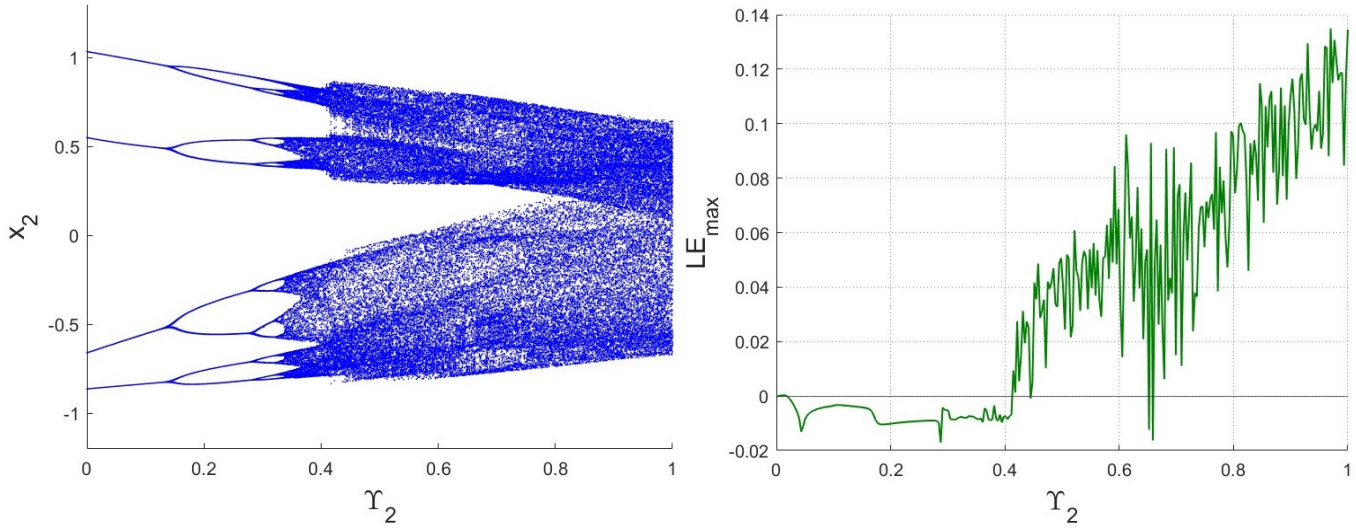

(**a**) (**b**)

Figure 11. (**a**) Bifurcation of (15) for $Y_2 \in (0, 1]$ and $Y_1 = 1$,$Y_3 = 0.9$. (**b**) The associated LE_{max}.

Figure 13 shows the bifurcation diagram for the incommensurate derivative $(Y_1, Y_2, Y_3) = (0.9, 0.1, 0.2)$, when $\sigma_1 \in [-1, 1]$, $\sigma_2 \in [-2, 0]$, $\sigma_3 \in [0, 1.2]$, $\eta \in [0, 1.5]$; obviously, the map changes the dynamics from periodic to totally chaotic and shows a divergence in the motion of infinity in some points where the LE_{max} in Figure 14 corresponds to Figure 13, further confirming these findings with fluctuations in the values in the range of positive and negative. It is obvious that the behaviors of the three proposed incommensurate map-based functions (15) are influenced by the system factors and variations in the incommensurate derivative have an influence on the dynamics of (15).

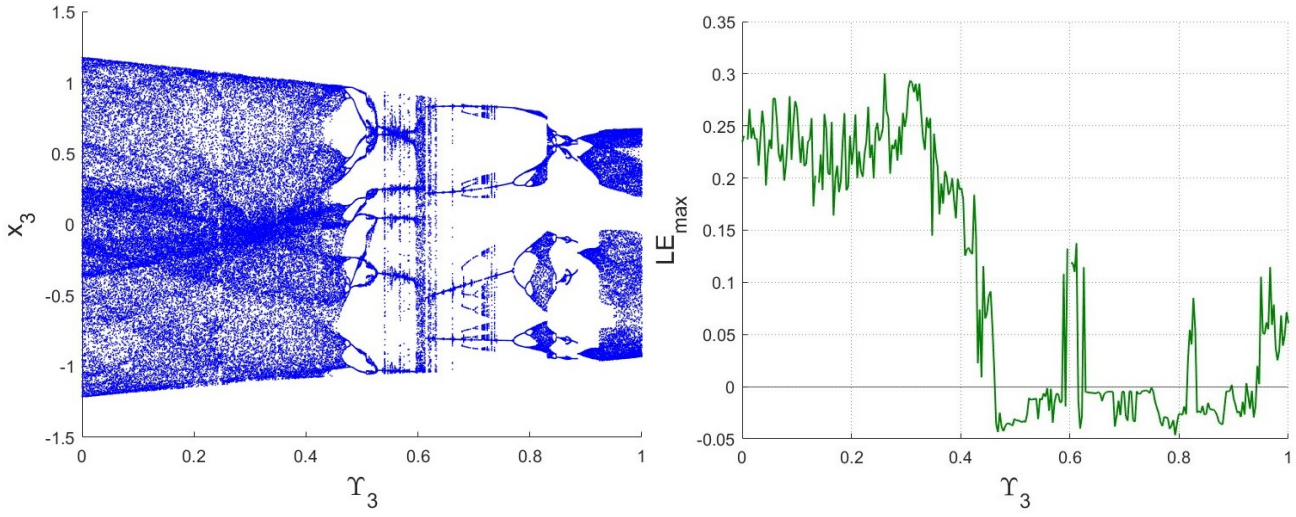

(**a**) (**b**)

Figure 12. (**a**) Bifurcation of (15) for $Y_3 \in (0, 1]$, $Y_1 = 0.9$, $Y_2 = 0.1$. (**b**) The associated LE_{max}.

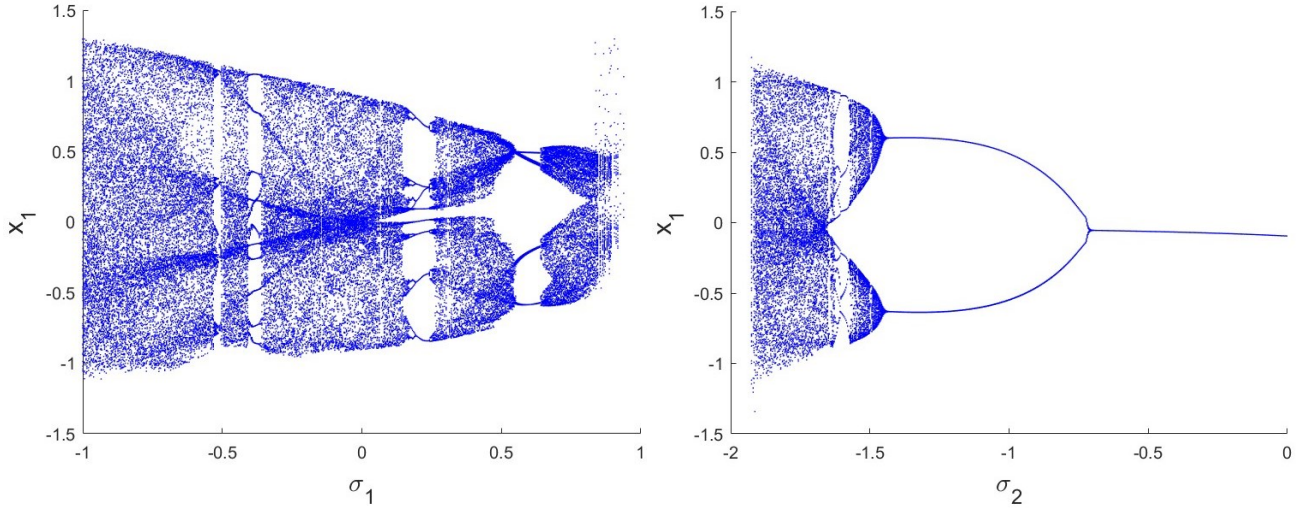

(**a**) $\sigma_1 \in [-1, 1]$ (**b**) $\sigma_2 \in [-2, 0]$

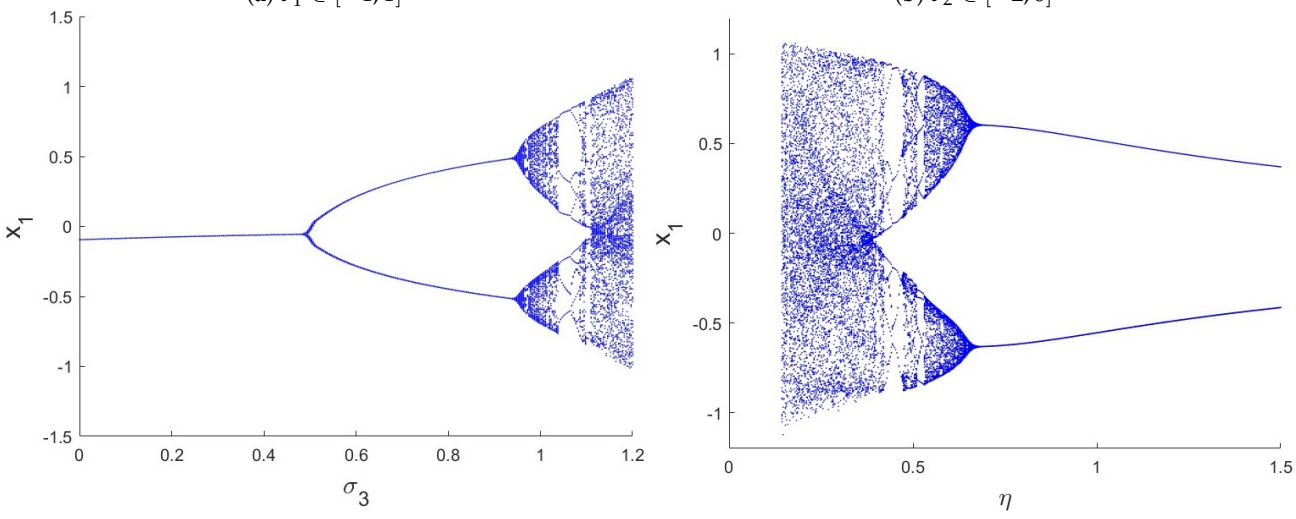

(**c**) $\sigma_3 \in [0, 1.2]$ (**d**) $\eta \in [0, 1.5]$

Figure 13. Bifurcation of (15) for $(Y_1, Y_2, Y_3) = (0.9, 0.1, 0.2)$.

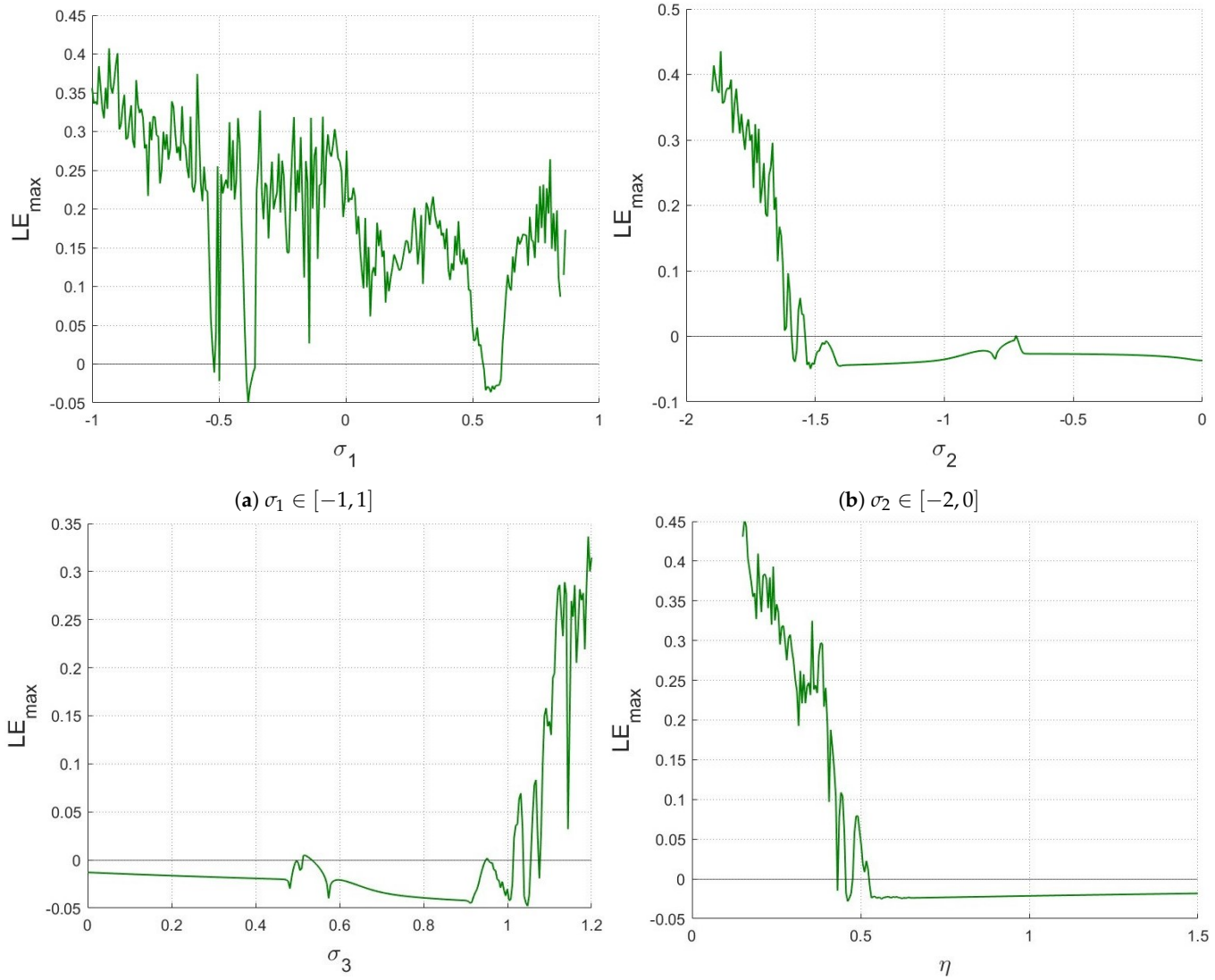

(**a**) $\sigma_1 \in [-1, 1]$ (**b**) $\sigma_2 \in [-2, 0]$

(**c**) $\sigma_3 \in [0, 1.2]$ (**d**) $\eta \in [0, 1.5]$

Figure 14. The LE_{max} of (15) associated with Figure 13.

4. Complexity Analysis

In this section, analyzing the dynamic of chaotic maps can also be performed using the complexity of chaotic features. As the complexity of the model increases, it becomes increasingly chaotic. The complexity of the new fractional-chaotic map-based three functions (9), (15) is ascertained using the C_0 measure and the approximate entropy $ApEn$ approach.

4.1. Entropy Test

In this part, the degree of complexity in the new fractional-chaotic maps-based three functions (9) and (15) in the time sequence created may be measured using the approximation entropy (ApEn) [36]. It corresponds to more chaotic behavior with higher ApEn. In theory, for $m = 2$, the embedding dimension of the ApEn algorithm is defined by

$$\mathbf{ApEn} = \Phi^m(r) - \Phi^{m+1}(r), \tag{17}$$

where $r = 0.2std(Z)$ is the tolerance so that $std(Z)$ is the standard deviation, and $\Phi^m(r)$ is noted as

$$\Phi^m(r) = \frac{1}{n-m+1} \sum_{\iota=1}^{n-m+1} \log C_\iota^m(r). \tag{18}$$

The $ApEn$ results for $\sigma_1 = -0.2$, $\sigma_2 = -1.7$, $\sigma_3 = 1.15$, $\beta = 1$, $\eta = 0.35$, and (IN) of the three commensurate map-based functions (9), as well as the incommensurate (15) when the values of commensurate and incommensurate orders are offered in Figure 15. Clearly, the higher values in the $ApEn$ findings indicate a higher level of chaos in the maps. This result thus validates the appearance of chaos in the maps (9), (15) and is consistent with the maximum Lyapunov exponent results previously shown in Figures 3 and 10–12.

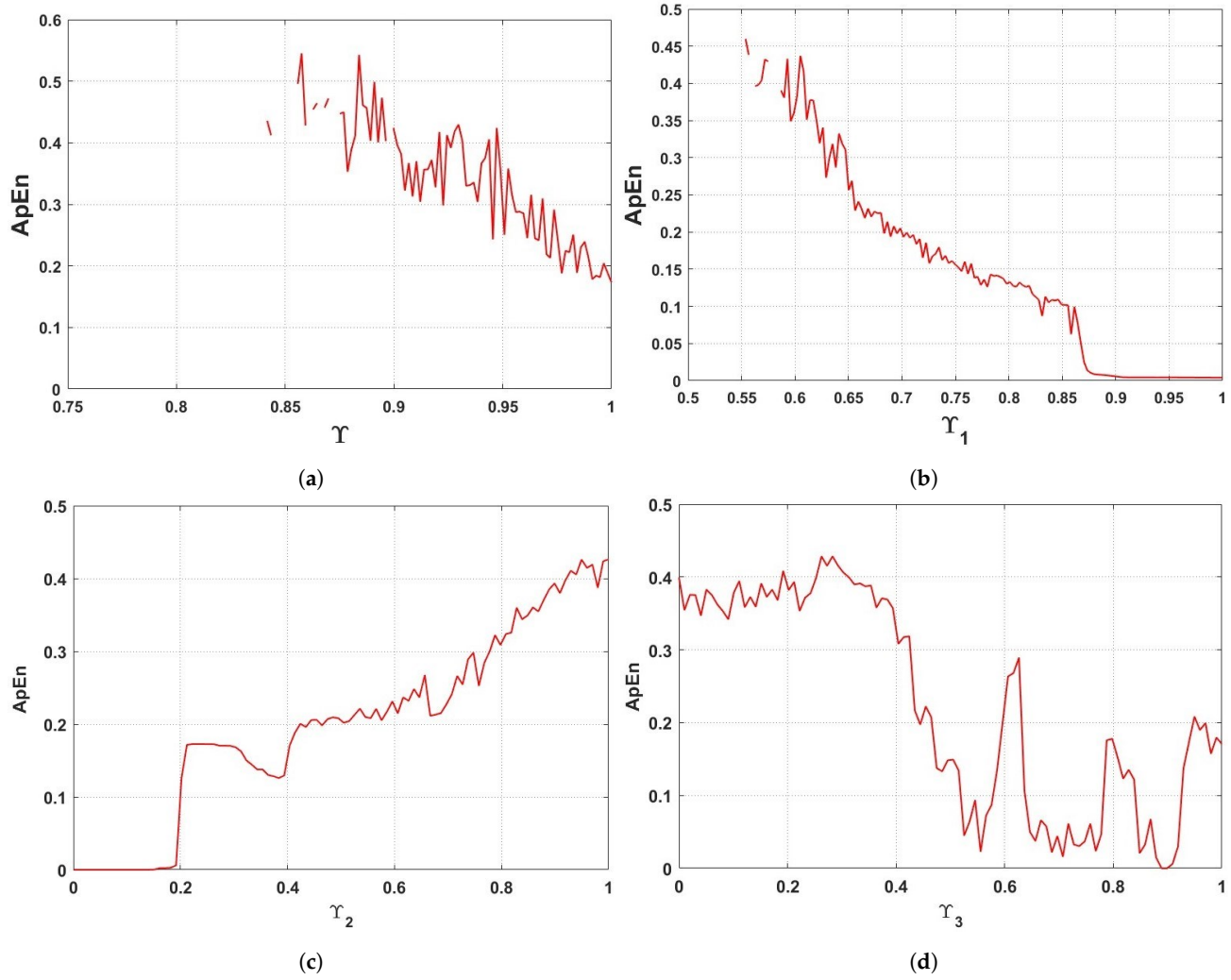

Figure 15. The $ApEn$ complexity of the maps (9) and (15) with (**a**) $\mathrm{Y} \in [0.65, 1]$, (**b**) $\mathrm{Y}_1 \in [0.4, 1]$ and $\mathrm{Y}_2 = 0.1$, $\mathrm{Y}_3 = 0.9$, (**c**) $\mathrm{Y}_2 \in (0, 1]$ and $\mathrm{Y}_1 = 1$,$\mathrm{Y}_3 = 0.9$, (**d**) $\mathrm{Y}_3 \in (0, 1]$ and $\mathrm{Y}_1 = 0.9$,$\mathrm{Y}_2 = 0.1$.

4.2. C_0 Complexity

Here, using the C_0 complexity algorithm [37], we calculate the complexity of the new fractional chaotic map-based three functions (9) and (15); this comes from the Fourier inverse transform. The C_0 algorithm is described in detail for $\{\phi(\gamma), \gamma = 1, \ldots, B-1\}$:

- $\phi(\gamma)$ is defined as the Fourier transform by

$$\mathbf{X}_B(\gamma) = \frac{1}{B} \sum_{\gamma=0}^{B-1} \phi(a) \exp^{-2\pi i(\frac{kj}{B})}, \quad a = 0, 1, \ldots, B-1. \tag{19}$$

- We detailed the mean square of $\mathbf{X}_B(\gamma)$ with $G_B = \frac{1}{B}\sum_{\gamma=0}^{N-1}|\mathbf{X}_B(\gamma)|^2$ and set

$$\bar{\mathbf{X}}_B(\gamma) = \begin{cases} \mathbf{X}_B(\gamma) & \text{if} \quad \|\mathbf{X}_B(\gamma)\|^2 > rG_B, \\ 0 & \text{if} \quad \|\mathbf{X}_B(\gamma)\|^2 \leq rG_B. \end{cases} \tag{20}$$

- The inverse Fourier transform may be found as

$$\xi(\jmath) = \frac{1}{B}\sum_{\gamma=0}^{B-1}\bar{\mathbf{X}}_B(\gamma)\exp^{2\pi i(\frac{\jmath\gamma}{B})}, \quad \jmath = 0, 1, \ldots, B-1. \tag{21}$$

- Applying the following formula yields the C_0 complexity

$$C_0 = \frac{\sum_{\jmath=0}^{B-1}\|\xi(\jmath) - \phi(\jmath)\|}{\sum_{\jmath=0}^{B-1}\|\phi(\jmath)\|^2}. \tag{22}$$

We evaluate C_0 complexity numerically for the new fractional chaotic map-based three functions (9) and (15), where $\sigma_1 = -0.2$, $\sigma_2 = -1.7$, $\sigma_3 = 1.15$, $\beta = 1$, $\eta = 0.35$, and (IN). Figure 16 illustrates changes in the derivative fractional orders Υ, Υ_1, Υ_2, and Υ_3. The maps exhibit more complexity, as shown by the higher C_0 complexity outcome. These results agree with (LE_{max}).

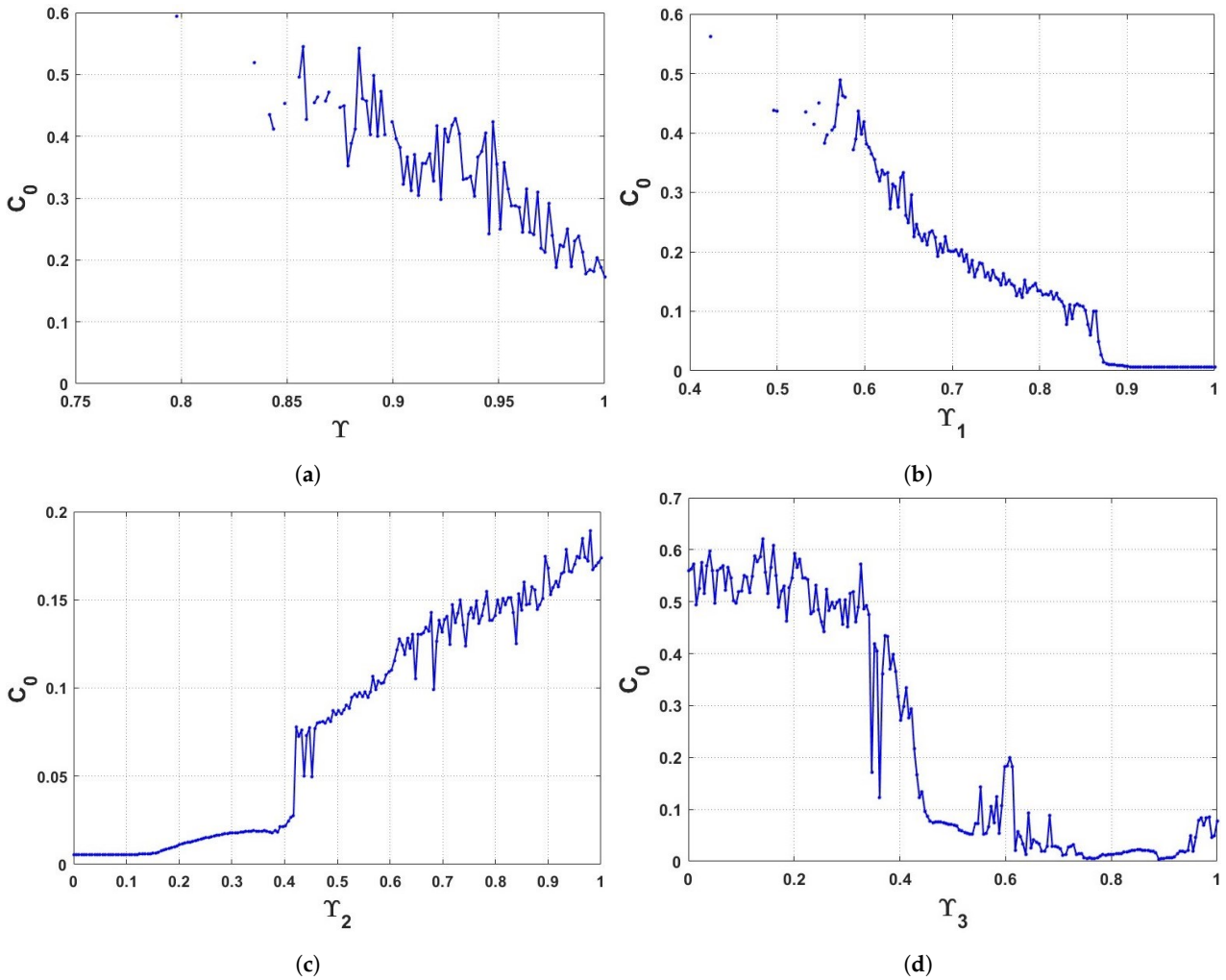

Figure 16. The C_0 complexity of the maps (9) and (15) with (**a**) $\Upsilon \in [0.65, 1]$, (**b**) $\Upsilon_1 \in [0.4, 1]$ and $\Upsilon_2 = 0.1$, $\Upsilon_3 = 0.9$, (**c**) $\Upsilon_2 \in [0, 1]$ and $\Upsilon_1 = 1$,$\Upsilon_3 = 0.9$, (**d**) $\Upsilon_3 \in [0, 1]$ and $\Upsilon_1 = 0.9$,$\Upsilon_2 = 0.1$.

5. Chaotic Control

Now, we suggest the control laws for stabilizing the three commensurate map-based functions (9) and the incommensurate map (15). This ensures that the map states are forced to zero in enough time.

5.1. Commensurate-Order Control

Here, we create an adaptive controller to stabilize the three commensurate map-based functions (9) and guarantee that every state approaches zero asymptotically. In [38], the authors described several properties of a nonlinear controller for fractional-order discrete-time chaotic systems, and particularly those driving all map states asymptotically toward zero. We achieve this objective based on the following Lemma.

Lemma 1 ([39]). *The following linear commensurate system has an asymptotically stable zero equilibrium*

$$ {}^{C}\Delta_{t}^{\Upsilon}\psi(m) = \boldsymbol{A}\psi(s-1+\Upsilon). \tag{23}$$

Let $\psi(s) = (\psi_1(s), ..., \psi_n(s))^T$, $0 < \Upsilon < 1$ *and* $\forall s \in \mathbb{N}_{t+1-\Upsilon}$. $\boldsymbol{A} \in R^{n\times n}$, *if*

$$\lambda_j \in \left\{ \rho \in \mathbb{C} : |\rho| < \left(2\cos\frac{|arg\rho| - \pi}{2-\Upsilon} \right)^{\Upsilon} \quad and \quad |arg\rho| > \frac{\Upsilon\pi}{2} \right\}, \tag{24}$$

for all λ_j *of* $\boldsymbol{A}$.

The controlled map of the commensurate order is defined by

$$\begin{cases} {}^{C}\Delta_{t}^{\Upsilon}x_1(s) = \dfrac{\sigma_1}{1+e^{-\beta x_1(\theta)}} + \sigma_2\sigma_3 x_1(\theta)(\eta|x_2(\theta)| - 1)((x_3(\theta))^2 - 1) \\ \qquad\qquad - x_1(\theta) + \mathbf{T}_1(\theta), \\ {}^{C}\Delta_{t}^{\Upsilon}x_2(s) = x_1(\theta) + \mathbf{T}_2(\theta), \\ {}^{C}\Delta_{t}^{\Upsilon}x_3(s) = \sigma_2 x_1(\theta)(\eta|x_2(\theta)| - 1) + \mathbf{T}_3(\theta), \end{cases} \tag{25}$$

where $(\mathbf{T}_1^*, \mathbf{T}_2^*, \mathbf{T}_3^*)^T$ is the adaptive controllers, based on Lemma 1, which can give the proposition below that designs the adaptive controller to control the commensurate-map-based three functions (9).

Proposition 1. *The following 3D control law can stabilize the commensurate map* (9)

$$\begin{cases} \boldsymbol{T}_1(\theta) = -\sigma_2\sigma_3 x_1(s-1+\Upsilon)(\eta|x_2(\theta)| - 1)((x_3(\theta))^2 - 1) - \\ \qquad \dfrac{\sigma_1}{1+e^{-\beta x_1(\theta)}}, \\ \boldsymbol{T}_2(\theta) = -\dfrac{1}{2}x_2(\theta) \\ \boldsymbol{T}_3(\theta) = -\sigma_2 x_1(\theta)(\eta|x_2(\theta)|) - \dfrac{1}{2}x_3(\theta). \end{cases} \tag{26}$$

Proof. Substituting (26) into (25), we obtain

$$ {}^{C}\Delta_{t}^{\Upsilon}\bar{X} = A\bar{X}(\theta), \tag{27}$$

where $\bar{X} = (x_1, x_2, x_3)^T$ and

$$\mathbf{A} = \begin{pmatrix} -1 & 0 & 0 \\ 1 & -\frac{1}{2} & 0 \\ 1.7 & 0 & -\frac{1}{2} \end{pmatrix}. \tag{28}$$

Therefore, the λ_j satisfies

$$|\lambda_J| < \left(2\cos\frac{|arg\lambda_J| - \pi}{2 - \mathrm{Y}}\right)^{\mathrm{Y}} \quad \text{and} \quad |\lambda_J| > \frac{\mathrm{Y}\pi}{2}.$$

Thus, the $(0, 0, 0)$ equilibrium of (26) is asymptotically stable. □

To display the results, numerical simulations were run with Proposition 1. Figure 17 displays the evolution of the controlled map (25) for $\mathrm{Y} = 0.85$, with $\sigma_1 = -0.2$, $\sigma_2 = -1.7$, $\sigma_3 = 1.15$, $\beta = 1$, $\eta = 0.35$, and (IN). Observably, the three commensurate map-based functions (9) are stabilized.

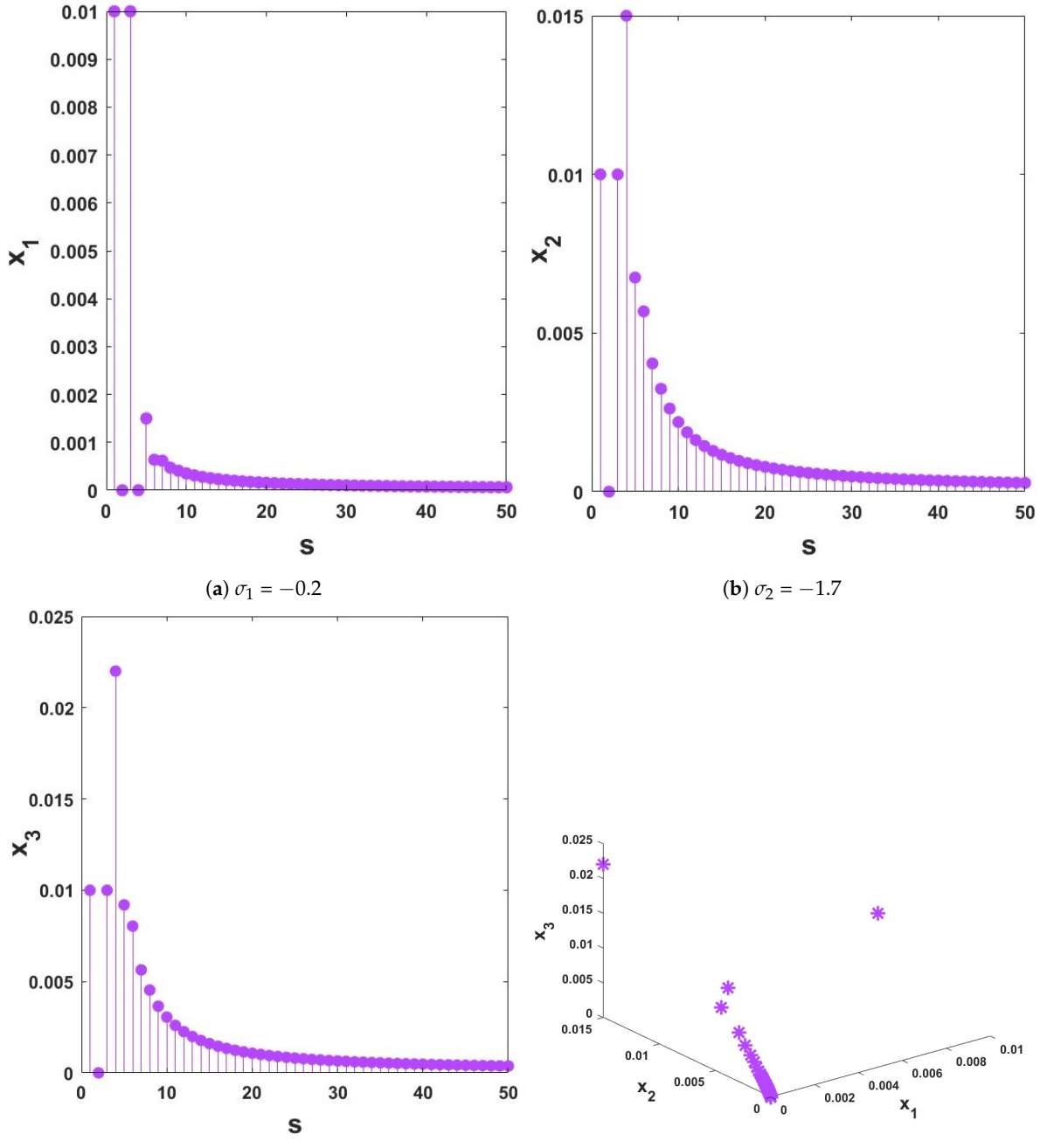

(**a**) $\sigma_1 = -0.2$ (**b**) $\sigma_2 = -1.7$

(**c**) $\sigma_3 = 1.15$ (**d**) Attractor

Figure 17. The evolution states of the controller three commensurate map-based functions (25) for $\mathrm{Y} = 0.85$.

5.2. Incommensurate-Order Control

In this part, we provide the stability requirement that every state converges to zero, thereby stabilizing the three proposed incommensurate map-based functions (15) using the following Lemma.

Lemma 2 ([40]). *Consider the system*

$$\begin{cases} {}^{c}\Delta_{t}^{\Upsilon_1} x_1(s) = \psi_1(x(\Upsilon_1 + s - 1)), \\ {}^{c}\Delta_{t}^{\Upsilon_2} x_2(s) = \psi_2(x(\Upsilon_2 + s - 1)), \qquad s = 0, 1, \cdots, \\ \quad \vdots \\ {}^{c}\Delta_{t}^{\Upsilon_m} x_m(s) = \psi_m(x(\Upsilon_m + s - 1)). \end{cases} \tag{29}$$

where $\psi = (\psi_1, ..., \psi_m) : \mathbb{R}^m \to \mathbb{R}^m$ *and* $x(s) = (x_1(s), ..., x_m(s))^T \in \mathbb{R}^m$*; consider* $\Upsilon_i \in (0, 1]$, $i = 1 \ldots m$*, and let* $\boldsymbol{M}$ *be (LCM) of the denominators* $\bar{\mu}_i$ *of* Υ_i *added to* $\Upsilon_i = \bar{u}_i \bar{\mu}_i$, $(\bar{\mu}_i, \bar{u}_i) = 1$, $\bar{u}_i, \bar{\mu}_i \in \mathbb{Z}_+$, $\forall i = \overline{1, m}$.

$$det(diag(\lambda^{\boldsymbol{M}\Upsilon_1}, \cdots, \lambda^{\boldsymbol{M}\Upsilon_m}) - (1 - \lambda^{\boldsymbol{M}})\boldsymbol{A}) = 0, \tag{30}$$

where $\boldsymbol{A}$ *is the Jacobian matrix of* (29)*. If each root of* (30) *is included in* $\mathbb{C}/K^{\delta}$*, the zero solution of* (29) *is asymptotically stable, where*

$$K^{\delta} = \left\{ \rho \in \mathbb{C} : |\rho| \leq \left(2\cos \frac{|arg\rho|}{\delta} \right)^{\delta} \quad and \quad |arg\rho| \leq \frac{\rho\pi}{2} \right\}, \tag{31}$$

and $\delta = \frac{1}{\boldsymbol{M}}$.

The controlled map of the incommensurate order is defined by

$$\begin{cases} {}^{C}\Delta_{t}^{\Upsilon_1} x_1(s) = \dfrac{\sigma_1}{1 + e^{-\beta x_1(\theta_1)}} + \sigma_2\sigma_3 x_1(\theta_1)(\eta|x_2(\theta_1)| - 1)((x_3(\theta_1))^2 - 1) \\ \qquad\qquad - x_1(\theta_1) + \mathbf{T}_1(\theta_1), \\ {}^{C}\Delta_{t}^{\Upsilon_2} x_2(s) = x_1(\theta_2) + \mathbf{T}_2(\theta_2), \\ {}^{C}\Delta_{t}^{\Upsilon_3} x_3(s) = \sigma_2 x_1(\theta_3)(\eta|x_2(\theta_3)| - 1) + \mathbf{T}_3(\theta_3), \end{cases} \tag{32}$$

Proposition 2. *The following 3D control law can stabilize the incommensurate map* (15)

$$\begin{cases} \boldsymbol{T}_1(\theta_1) = -\sigma_2\sigma_3 x_1(\theta_1)(\eta|x_2(\theta_1)| - 1)((x_3(\theta_1))^2 - 1) - \\ \qquad \dfrac{\sigma_1}{1 + e^{-\beta x_1(\theta_1)}}, \\ \boldsymbol{T}_2(\theta_2) = -\dfrac{1}{2} x_2(\theta_2), \\ \boldsymbol{T}_3(\theta_3) = -\sigma_2 x_1(\theta_3)(\eta|x_2(\theta_3)|) - \dfrac{1}{2} x_3(\theta_3). \end{cases} \tag{33}$$

Proof. Substituting (33) into (32) we get:

$$\begin{cases} {}^{C}\Delta_{t}^{\Upsilon_1} x_1(s) = -x_1(\theta_1), \\ {}^{C}\Delta_{t}^{\Upsilon_2} x_2(s) = x_1(\theta_2) - \dfrac{1}{2} x_2(\theta_2), \\ {}^{C}\Delta_{t}^{\Upsilon_3} x_3(s) = -\sigma_2 x_1(\theta_3) - \dfrac{1}{2} x_3(\theta_3). \end{cases} \tag{34}$$

So,

$$det(diag(\lambda^{\mathbf{M}Y_1}, \lambda^{\mathbf{M}Y_2}, \lambda^{\mathbf{M}Y_3})) - (1 - \lambda^{\mathbf{M}})A) = 0$$

where $\mathbf{M} = 10$, and

$$\mathbf{A} = \begin{pmatrix} -1 & 0 & 0 \\ 1 & -\frac{1}{2} & 0 \\ 1.7 & 0 & -\frac{1}{2} \end{pmatrix}, \tag{35}$$

for $(Y_1, Y_2, Y_3) = (1, 0.8, 0.9)$

$$\det\left(\begin{pmatrix} \lambda^1 & 0 & 0. \\ 0 & \lambda^8 & 0 \\ 0 & 0 & \lambda^9 \end{pmatrix} - \left(1 - \lambda^{10}\right)\mathbf{A}\right) = 0,$$

$\Leftrightarrow$

$$-0.25\lambda^{30} + 0.5\lambda^{29} + 0.5\lambda^{28} - \lambda^{27} + 0.25\lambda^{21} + 0.25\lambda^{20} - 1.5\lambda^{19} + \lambda^{17} - 0.5\lambda^{11} - 0.25\lambda^{10} + \lambda^9 + 0.5\lambda^8 + 0.25\lambda + 0.25 = 0. \tag{36}$$

Based on Lemma 2, realizing that $\lambda_j \in \mathbb{C}/K^{\frac{1}{10}}$, $(j = 1, \ldots, 30)$, which the map (32) asymptotically stabilizes towards $(0, 0, 0)$ equilibrium. □

In Figure 18, display the stabilization of controller map (32) for $(Y_1, Y_2, Y_3) = (1, 0.8, 0.9)$ with (IN). Hence, we can see that the three new incommensurate map-based functions (15) are stabilized.

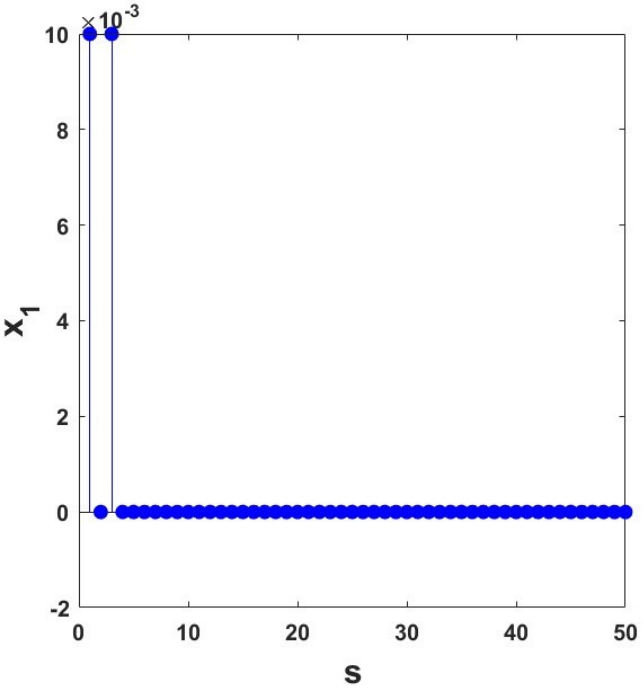

(**a**) $Y_1 = 1$

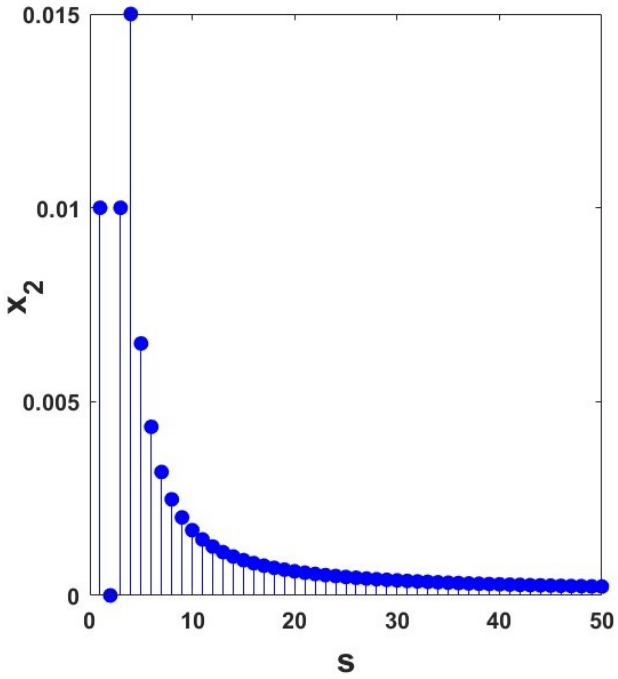

(**b**) $Y_2 = 0.8$

Figure 18. *Cont.*

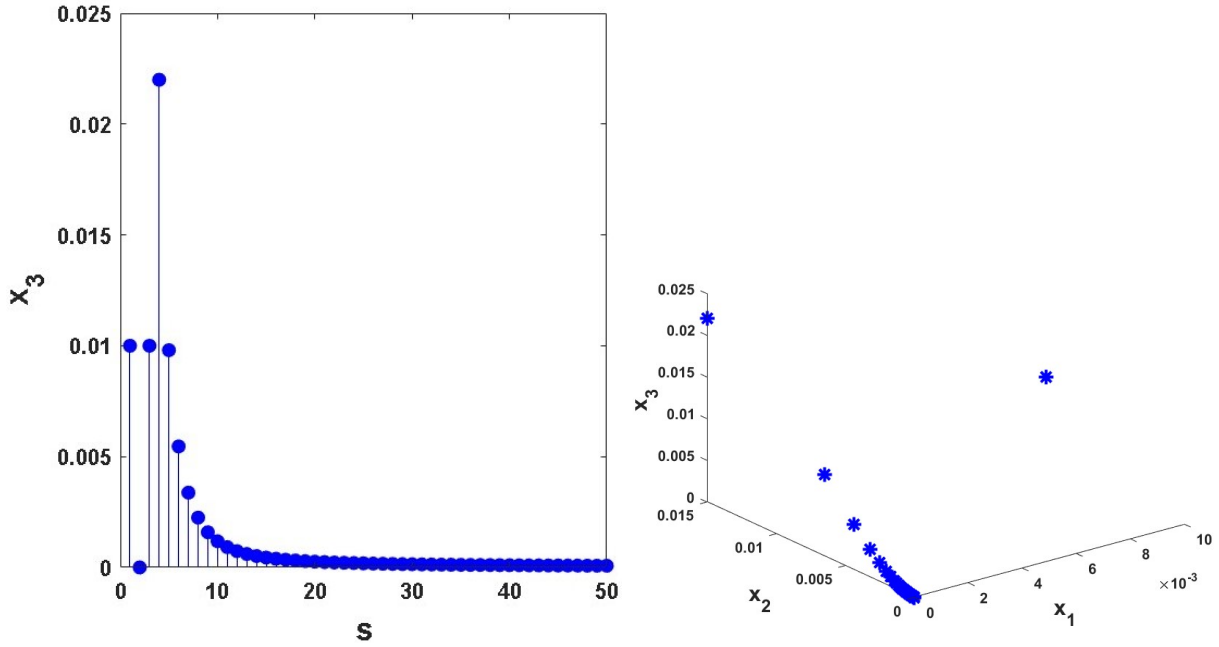

(**c**) $Y_3 = 0.9$ (**d**) Attractor

Figure 18. The evolution states of the controller's three incommensurate map-based functions (32) for $(Y_1, Y_2, Y_3) = (1, 0.8, 0.9)$.

6. Conclusions and Future Works

A new fractional chaotic map-based three functions are introduced, and we thoroughly investigated their dynamics in commensurate as well as incommensurate derivative orders, adding to their influence on the map's behavior. Our work provides significant insights into the intricate dynamics of discrete systems based on nonlinear functions under fractional orders through this method, paving the way for further study and real-world applications in the fields of nonlinear dynamics and chaos theory.

First, the analysis of the system with no fixed point also varied the parameters and derivative fractional values, revealing that there is asymmetry, further highlighting that the system is able to display a wide range of complex hidden dynamical behaviors. Second, the approximation entropy $ApEn$ and C_0 complexity confirmed the quantitative assessment of the system's complexity. Third, producing effective control laws can force the new fractional chaotic map-based three function states to approach asymptotic zero and guarantee their stabilization.

Lastly, numerical simulations with MATLAB R2024a are run to illustrate the results. Such a phenomenon in encryption and secure communication maps based on mathematical functions will be used in subsequent work. So, we will be designing relevant physical device realizations to validate the numerical simulation results.

Author Contributions: Conceptualization, M.A.H. and M.A.; data curation, H.A.-T. and A.O.; formal analysis, M.A. and L.D.; funding acquisition, H.A.-T., M.A.H. and M.A.; investigation, A.O.; methodology, L.D.; project administration, M.A.H.; resources, H.A.-T. and M.A.H.; software, L.D. and A.O.; supervision, M.A.H.; validation, M.A.; visualization, A.O.; writing—original draft, L.D.; writing—review and editing, H.A.-T., M.A. and A.O. All authors have read and agreed to the published version of the manuscript.

Funding: This research received no external funding.

Data Availability Statement: The original contributions presented in the study are included in the article, further inquiries can be directed to the corresponding author.

Conflicts of Interest: The authors declare no conflicts of interest.

References

1. Siregar, E.; Mawengkang, H.; Nababan, E.B.; Wanto, A. Analysis of Backpropagation Method with Sigmoid Bipolar and Linear Function in Prediction of Population Growth. *J. Phys. Conf. Ser.* **2019**, *1255*, 1. [CrossRef]
2. Martinelli, C.; Coraddu, A.; Cammarano, A. Approximating piecewise nonlinearities in dynamic systems with sigmoid functions: Advantages and limitations. *Nonlinear Dyn.* **2023**, *111*, 8545–8569. [CrossRef]
3. Erkan, U.; Toktas, A.; Lai, Q. Design of two dimensional hyperchaotic system through optimization benchmark function. *Chaos Solitons Fractals* **2023**, *167*, 113032. [CrossRef]
4. Baione, F.; Biancalana, D.; De Angelis, P. An application of Sigmoid and Double-Sigmoid functions for dynamic policyholder behaviour. *Decis. Econ. Financ.* **2021**, *44*, 5–22. [CrossRef]
5. Mfungo, D.E.; Fu, X.; Wang, X.; Xian, Y. Enhancing image encryption with the Kronecker Xor product, the Hill Cipher, and the Sigmoid Logistic Map. *Appl. Sci.* **2023**, *13*, 4034. [CrossRef]
6. Jiang, H.G.; Jia, M.M. Chaos control for multi-scroll chaotic attractors generated by introducing a bipolar sigmoid function series. *Indian J. Phys.* **2020**, *94*, 851–861. [CrossRef]
7. Hamadneh, T.; Hioual, A.; Alsayyed, O.; Al-Khassawneh, Y.A.; Al-Husban, A.; Ouannas, A. The FitzHugh–Nagumo Model Described by Fractional Difference Equations: Stability and Numerical Simulation. *Axioms* **2023**, *12*, 806. [CrossRef]
8. Almatroud, O.A.; Abu Hammad, M.M.; Dababneh, A.; Diabi, L.; Ouannas, A.; Khennaoui, A.A.; Alshammari, S. Multistability, Chaos, and Synchronization in Novel Symmetric Difference Equation. *Symmetry* **2024**, *16*, 1093. [CrossRef]
9. Khennaoui, A.A.; Ouannas, A.; Bendoukha, S.; Grassi, G.; Wang, X.; Pham, V.T.; Alsaadi, F.E. Chaos, control, and synchronization in some fractional-order difference equations. *Adv. Differ. Equ.* **2019**, *2019*, 412. [CrossRef]
10. Hammad, M.M.A.; Diabi, L.; Dababneh, A.; Zraiqat, A.; Momani, S.; Ouannas, A.; Hioual, A. On New Symmetric Fractional Discrete-Time Systems: Chaos, Complexity, and Control. *Symmetry* **2024**, *16*, 840. [CrossRef]
11. Marwan, M.; Han, M.; Dai, Y.; Cai, M. The Impact of Global Dynamics on the Fractals of a Quadrotor Unmanned Aerial Vehicle (Quav) Chaotic System. *Fractals* **2024**, *32*, 2450043. [CrossRef]
12. Zhang, D.; Li, F. Chaotic Dynamics of Non-Autonomous Nonlinear System for a Sandwich Plate with Truss Core. *Mathematics* **2022**, *10*, 1889. [CrossRef]
13. Abdeljawad, T.; Sher, M.; Shah, K.; Sarwar, M.; Amacha, I.; Alqudah, M.; Al-Jaser, A. Analysis of a class of fractal hybrid fractional differential equation with application to a biological model. *Sci. Rep.* **2024**, *14*, 18937. [CrossRef]
14. Ahmadi, A.; Parthasarathy, S.; Pal, N.; Rajagopal, K.; Jafari, S.; Tlelo-Cuautle, E. Extreme multistability and extreme events in a novel chaotic circuit with hidden attractors. *Int. J. Bifurc. Chaos* **2022**, *33*, 2330016. [CrossRef]
15. Leutcho, G.D.; Wang, H.; Kengne, R.; Kengne, L.K.; Njitacke, Z.T.; Fozin, T.F. Symmetry-breaking, amplitude control and constant Lyapunov exponent based on single parameter snap flows. *Eur. Phys. J. Spec. Top.* **2022**, *230*, 1887–1903. [CrossRef]
16. Azar, A.T.; Vaidyanathan, S.; Ouannas, A. *Fractional Order Control and Synchronization of Chaotic Systems*; Springer: Berlin/Heidelberg, Germany, 2017; Volume 688, pp. 154–196.
17. Jiang, C.; Zada, A.; Şenel, M.T.; Li, T. Synchronization of bidirectional N-coupled fractional-order chaotic systems with ring connection based on antisymmetric structure. *Adv. Differ. Equ.* **2019**, *2019*, 456. [CrossRef]
18. Jiang, C.; Zhang, F.; Li, T. Synchronization and antisynchronization of N-coupled fractional-order complex chaotic systems with ring connection. *Math. Methods Appl. Sci.* **2018**, *41*, 2625–2638. [CrossRef]
19. Chen, X.; Park, J.H.; Cao, J.; Qiu, J. Sliding mode synchronization of multiple chaotic systems with uncertainties and disturbances. *Appl. Math. Comput.* **2017**, *308*, 161–173. [CrossRef]
20. Xia, Y.; Wang, J.; Meng, B.; Chen, X. Further results on fuzzy sampled-data stabilization of chaotic nonlinear systems. *Appl. Math. Comput.* **2020**, *379*, 125225. [CrossRef]
21. Hamadneh, T.; Abbes, A.; Al-Tarawneh, H.; Gharib, G.M.; Salameh, W.M.M.; Al Soudi, M.S.; Ouannas, A. On chaos and complexity analysis for a new sine-based memristor map with commensurate and incommensurate fractional orders. *Mathematics* **2023**, *11*, 4308. [CrossRef]
22. Qin, H.; Gu, Z.; Fu, Y.; Li, T. Existence of mild solutions and controllability of fractional impulsive integrodifferential systems with nonlocal conditions. *J. Funct. Spaces* **2017**, *2017*, 6979571. [CrossRef]
23. Elaskar, S. Symmetry in Nonlinear Dynamics and Chaos. *Symmetry* **2022**, *15*, 102. [CrossRef]
24. Karimov, T.; Rybin, V.; Kolev, G.; Rodionova, E.; Butusov, D. Chaotic communication system with symmetry-based modulation. *Appl. Sci.* **2021**, *11*, 3698. [CrossRef]
25. Wang, R.; Li, C.; Kong, S.; Jiang, Y.; Lei, T. A 3D memristive chaotic system with conditional symmetry. *Chaos Solitons Fractals* **2022**, *158*, 111992. [CrossRef]
26. Pratiwi, H.; Windarto, A.P.; Susliansyah, S.; Aria, R.R.; Susilowati, S.; Rahayu, L.K.; Fitriani, Y.; Merdekawati, A.; Rahadjeng, I.R. Sigmoid activation function in selecting the best model of artificial neural networks. *J. Phys. Conf. Ser.* **2020**, *1471*, 012010. [CrossRef]
27. Yang, Y.; Huang, L.; Xiang, J.; Bao, H.; Li, H. Design of multi-wing 3D chaotic systems with only stable equilibria or no equilibrium point using rotation symmetry. *AEU-Int. J. Electron. Commun.* **2021**, *135*, 153710. [CrossRef]
28. Lin, H.; Wang, C.; Sun, J.; Zhang, X.; Sun, Y.; Iu, H.H. Memristor-coupled asymmetric neural networks: Bionic modeling, chaotic dynamics analysis and encryption application. *Chaos Solitons Fractals* **2023**, *166*, 112905. [CrossRef]

29. Xu, Q.; Cheng, S.; Ju, Z.; Chen, M.; Wu, H. Asymmetric coexisting bifurcations and multi-stability in an asymmetric memristive diode-bridge-based jerk circuit. *Chin. J. Phys.* **2021**, *70*, 69–81. [CrossRef]
30. Atici, F.M.; Eloe, P. Discrete fractional calculus with the nabla operator. *Electron. J. Qual. Theory Differ. Equ. [Electron. Only]* **2009**, *62*, 12. [CrossRef]
31. Abdeljawad, T. On Riemann and Caputo fractional differences. *Comput. Math. Appl.* **2011**, *62*, 1602–1611. [CrossRef]
32. Wu, G.C.; Baleanu, D. Discrete fractional logistic map and its chaos. *Nonlinear Dyn.* **2014**, *75*, 283–287. [CrossRef]
33. Thoai, V.P.; Pham, V.T.; Grassi, G.; Momani, S. Assessing sigmoidal function on memristive maps. *Heliyon* **2024**, *10*, e27781. [CrossRef] [PubMed]
34. Anastassiou, G.A. General multiple sigmoid functions relied complex valued multivariate trigonometric and hyperbolic neural network approximations. *RGMIA Res. Rep. Coll.* **2023**, *26*, 43.
35. Wu, G.C.; Baleanu, D. Jacobian matrix algorithm for Lyapunov exponents of the discrete fractional maps. *Commun. Nonlinear Sci. Numer. Simul.* **2015**, *22*, 95–100. [CrossRef]
36. Richman, J.S.; Moorman, J.R. Physiological time-series analysis using approximate entropy and sample entropy. *Am. J.-Physiol.-Heart Circ. Physiol.* **2000**, *278*, H2039–H2049. [CrossRef]
37. Shen, E.-h.; Cai, Z.-j.; Gu, F.-j. Mathematical foundation of a new complexity measure. *Appl. Math. Mech.* **2005**, *26*, 1188–1196.
38. Ouannas, A.; Batiha, I.M.; Pham, V.T. *Fractional Discrete Chaos: Theories, Methods and Applications*; World Scientific: Singapore, 2023; Volume 3, pp. 1–300.
39. Čermák, J.; Győri, I.; Nechvátal, L. On explicit stability conditions for a linear fractional difference system. *Electron. J. Qual. Theory Differ. Equ. [Electron. Only]* **2015**, *18*, 651–672. [CrossRef]
40. Shatnawi, M.T.; Djenina, N.; Ouannas, A.; Batiha, I.M.; Grassi, G. Novel convenient conditions for the stability of nonlinear incommensurate fractional-order difference systems. *Alex. Eng. J.* **2022**, *61*, 1655–1663. [CrossRef]